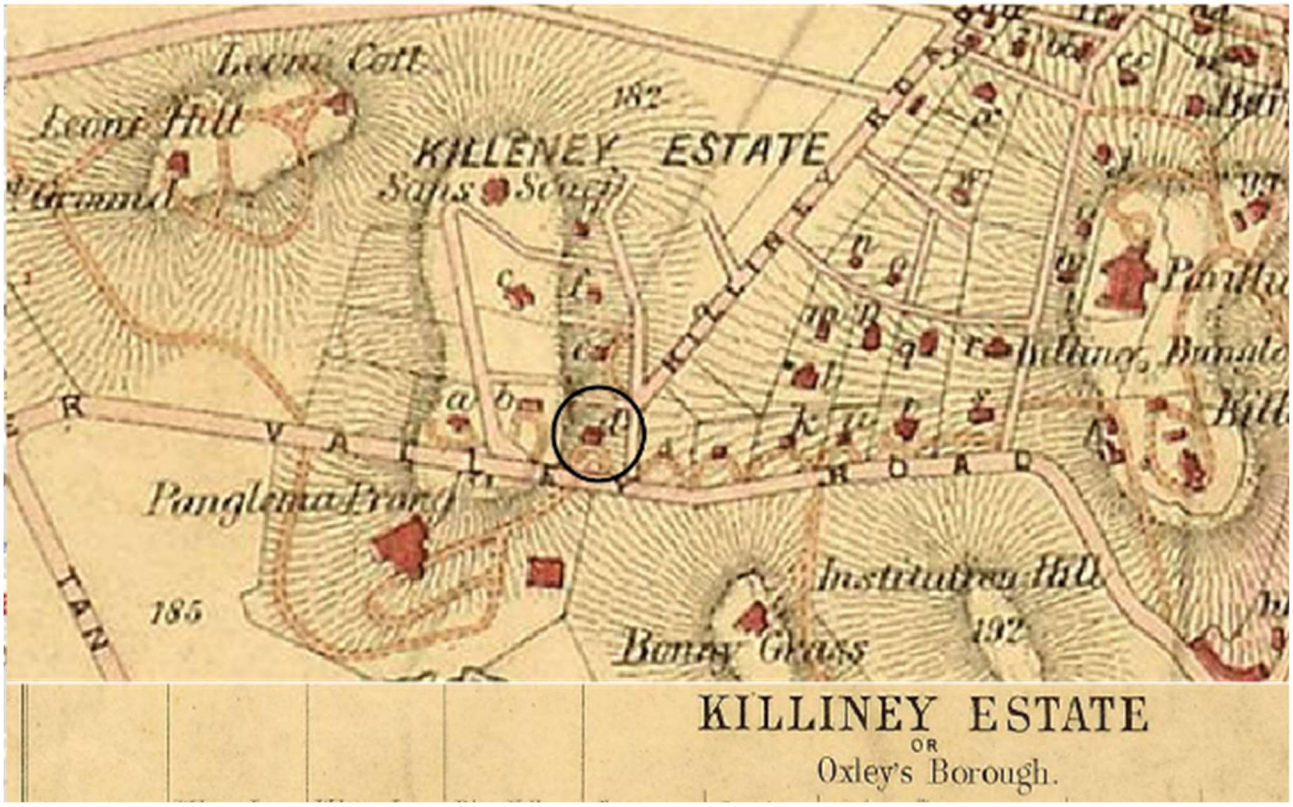

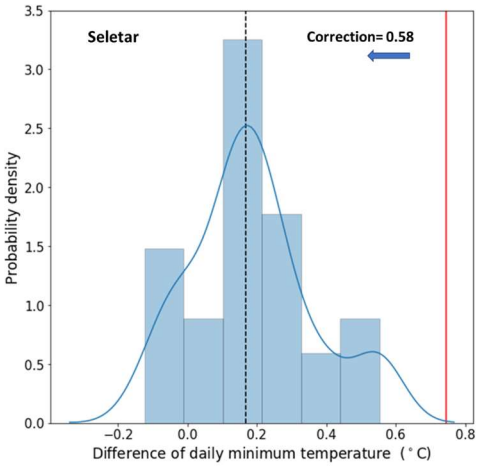

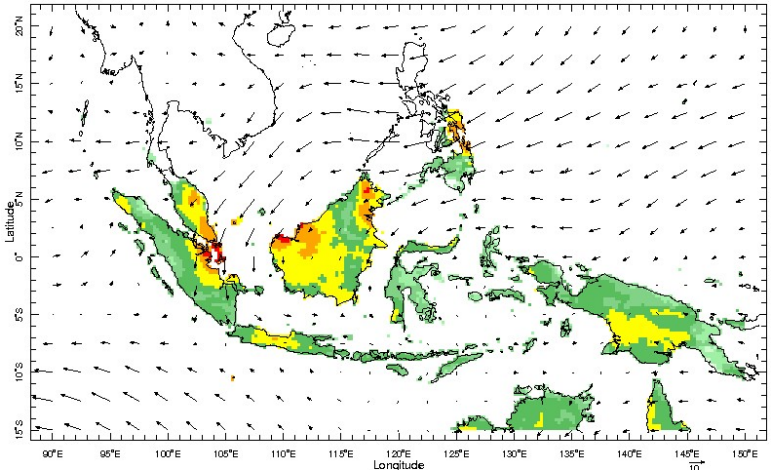

MSS RESEARCH LETTERS

Issue #2, December 2018

METEOROLOGICAL SERVICE SINGAPORE

DISCLAIMER OF WARRANTIES AND LIABILITY

1. While National Environment Agency Meteorological Service Singapore (NEA MSS) has made every reasonable effort to ensure that the information contained in this publication has been obtained from reliable sources, NEA MSS shall not be responsible for any errors or omissions, or for the results obtained from the use of such information.

2. NEA MSS shall also not be liable for any damage or loss of any kind howsoever caused as a result of any reliance on the contents of this publication.

EDITOR'S NOTE

I am pleased to present the second issue of MSS Research Letters. Following up from the inaugural May 2018 issue, this December issue includes a new set of scientific contributions from Meteorological Service Singapore, several written in collaboration with researchers from other institutes (National University of Singapore, Singapore Management University, MetService New Zealand, and Universiti Sains Malaysia). It is gratifying to see these collaborations, and it is my hope that MSS Research Letters will continue to publish collaborative works in the future.

As with the first issue, many of the contributions in this issue focus on rainfall – highlighting its importance to the region. The first contribution extends Singapore's longest rainfall record back to 1839, from which further study on climate variability can be undertaken. The impact of the Madden Julian Oscillation—a key driver of week to week variation in the Maritime Continent— on heavy rainfall over the seasons is also investigated. Building on this week-to-week variability, the third contribution considers four flood events on the Malay Peninsula and whether the associated heavy rainfall could have been predicted up to four weeks before the event. Rounding out the rainfall-related letters, a new 'nowcasting' system to forecast heavy rainfall for the next hour over Singapore is also tested. However, rainfall is not the sole meteorological variable investigated; the last contribution investigates the remarkable January 2018 cold spell in the historical context.

Once again, I would like to thank all the reviewers for their time and effort in improving these letters. A big thank you must also go to our external reviewers for this issue: Chris Gordon, Debora Hudson, Roberto Buizza, and Winston Chow. Your contribution to ensure the scientific integrity of the MSS Research Letters and your guidance to improve these letters and MSS Research Letters in general is much appreciated.

To all our readers, both inside and outside Meteorological Service Singapore, we hope you enjoy this issue of MSS Research Letters and will consider submitting suitable material for subsequent issues.

Warm regards,
Thea Turkington
Editor, MSS Research Letters

Cover figures: top – Historical map of Killiney Estate with location of rainfall station (Creating Singapore's longest monthly rainfall record from 1839 to the present, page 6); bottom left – Differences in daily mean minimum temperature at Seletar station (Was the Singapore January 2018 cold spell record-breaking? page 27); bottom right – Average daily precipitation during Jan 2004 flood event (Subseasonal forecasting of major wet spells in the southern Malay Peninsula, page 20)

TABLE OF CONTENTS

CREATING SINGAPORE'S LONGEST MONTHLY RAINFALL RECORD FROM 1839 TO THE PRESENT

Elaine Gao[1], Bertrand Timbal[1], Fiona Williamson[2],

[1]Climate Modelling and Prediction Section, Centre for Climate Research Singapore, [2]School of Social Sciences, Singapore Management University

INTRODUCTION

Rainfall in Singapore is highly variable on inter-annual and multi-decadal timescales. While annual rainfall had increased over the past 30 years until 2012 and has been decreasing more recently, year-to-year variations dominate observed trends and are therefore not statistically significant (Figure 1a). Similarly, future climate projections for Singapore are inconclusive about future trend of annual rainfall (Marzin et al. 2015). Improved understanding of natural variability on long time-scales can significantly reduce uncertainty in future climate projections. Currently, the identification of decadal variability is limited by the lack of long-term meteorological datasets; Singapore's reliable contemporary network of automatic meteorological stations (AWS) provides about 30 years of rainfall data for the whole island. Besides the modern network of AWS (Figure 2), an important historical time series has been the official single-station records from MacRitchie station, which extend as far back as 1879, providing 138 years of monthly rainfall data. This time series will be useful to evaluate long-term multi-decadal variability in this part of the world and potentially in most of the tropics.

Newly-discovered observations from historical archives and unofficial sources offer the possibility to extend records further back to 1839. This long-term record, unique to Singapore, is particularly exciting considering the dearth of historical meteorological data typical of other tropical countries (Nash and Adamson 2014). In this study, rainfall data pre-dating the start of official MacRitchie observations (1879), are compiled from various locations across the island. By making use of the contemporary AWS network, the current spatial relationships of rainfall between the historical sites and the current MacRitchie site are evaluated. Historical rainfall at MacRitchie from 1839–present is then reconstructed using the archive data, building a single-location, extended rainfall record (though discontinuous). In the process, the reliability of the official MacRitchie record is also examined, which is comprised of two separate data sources.

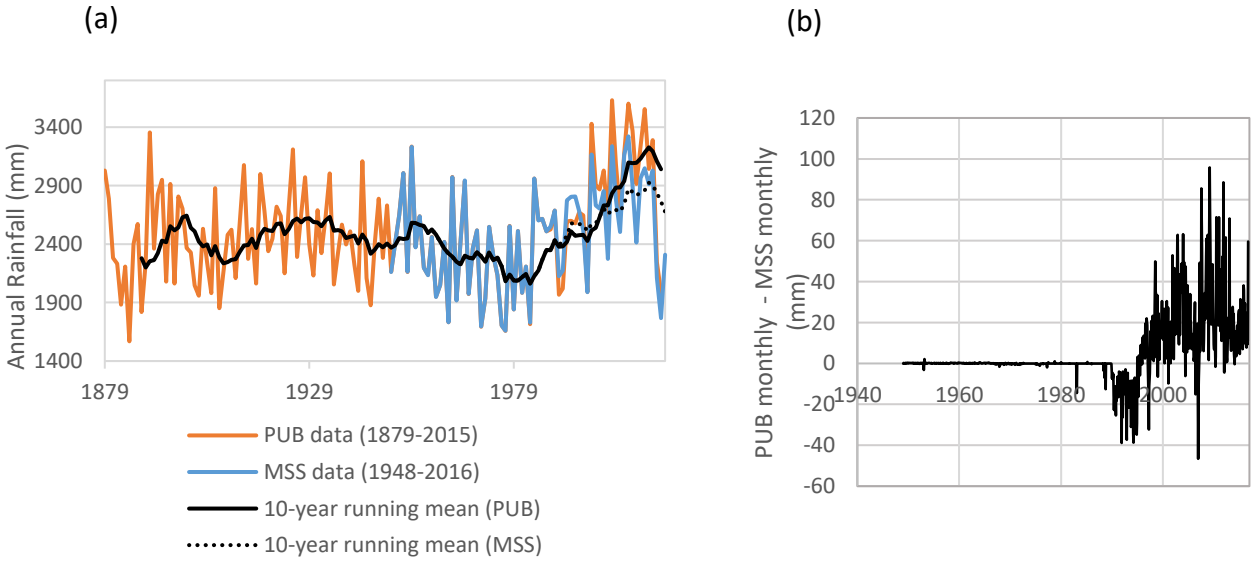

Figure 1 (a) Current long-term annual rainfall record for MacRitchie station, composite of data from the rain gauge managed by the Singapore's National Water Agency (PUB) and by the Meteorological Service Singapore (MSS). Both gauges are located at MacRitchie Reservoir and are situated within 5 m of each other. The differences in monthly values between PUB and MSS over time are in (b).

DATA

Three types of monthly rainfall data were used in this study: (1) current long-term records from MacRitchie station (1879–2016), (2) historical observations of rainfall compiled from various sources (1839–1883), and (3) contemporary 28-station record (1980–2014). Datasets (1) and (2) are detailed below.

(1) OFFICIAL LONG-TERM MACRITCHIE STATION RECORDS (1879–2016)

Presently, there are two rain gauges located immediately adjacent to each other in the MacRitchie station site near Pumping Station 1. To the authors' knowledge the gauges have not moved since their respective installation, though there remains some dispute on this matter (Saw and Ang, personal communication 2018). The instruments are managed by two separate agencies in Singapore, and hence two different MacRitchie datasets exist. Observations from the instrument currently managed by the Singapore's National Water Agency (PUB) are available from 1879—present [1], whilst observations from the instrument managed by the Meteorological Service Singapore (MSS) are available from 1948—present (Figure 1a). Rainfall totals for four months (October 1892, January 1942, January and February 1947) are missing from the PUB dataset. These have been replaced by 30-year centred-means for each particular month.

When comparing the PUB and MSS time series, it is apparent that the magnitudes of differences in the monthly totals between the two records are notably different before and after 1989 (Figure 1b). From 1948–1989, there is a near perfect correspondence between the two gauges, with most differences at 0.9 mm or less, possibly due to different rounding approaches, human error, or a combination of both. Monthly differences in excess of 1 mm were observed on 10 occasions: February and March 1953, December 1967, November 1975, April 1977, October 1978, February 1983 (the largest monthly difference at 14.5 mm), as well as June, August, and October 1988. Some of these may be due to the inconsistent reporting of the start or end of the month (e.g. February 1953 the MSS time series is 3.2 mm higher, and March 1953 the PUB is 2.1 mm higher, leading to the possibility that the end of February rainfall recorded by MSS may have been included in the March PUB time series). Given the similarity between the two time series, it is likely that during this period the same instrument was used by both agencies to compile their monthly statistics. Unfortunately, it is difficult with the existing metadata to identify the source of the differences between the two time series.

Table 1 Timeline of instrument changes for MacRitchie rain gauge managed by PUB and MSS respectively.

Date	PUB Instrument	Date	MSS Instrument
1879–1953	Simple manual gauge; only monthly records available from PUB from 1879 – 1948 (though daily readings were available, see footnote 1). Daily records available from 1949–present.		
1954–1983	Autographic recorder system installed; (daily) strip charts manually read.	1948–25 May 1982	Natural siphon gauge.
1984–1994	Tipping bucket rain gauge; monthly rainfall charts generated.	26 May 1983–7 May 1987	Dines tilting siphon gauge.
1995–present	Electronic data logging system installed.	8 May 1987–12 Feb 2009	Hellman recorder installed.
		13 Feb 2009–present	3G tipping bucket recorder installed. Comparison of rainfall measured from old and new MSS gauges were done for 13 months after installation to ensure consistency of instrument measurements. Measurements from new gauge logged from May 2010 onwards.

[1]Prior to the establishment of PUB in 1963, the Municipal Committee or Municipal Commission, managed the water supply from MacRitchie reservoir. Daily rainfall measurements were made by the Municipal Engineer, with the earliest known reference published in The Straits Times (7 Sep 1878), detailing the daily rainfall for Aug 1878, pre-dating the official record kept by PUB. Unfortunately, the complete dataset from the Municipal Committee was never published in The Straits Times. The Aug 1878 monthly total is consistent with the Global Historical Climatology Network (GHCN-Monthly) Version 2 dataset for MacRitchie station, the latter of which extends as far back as 1875.

From January 1990, a pronounced wet-bias for the MSS record in comparison to the PUB record is observed, suggesting that from 1990 onwards two different instruments were in use at the adjacent MSS and PUB sites. This wet-bias in the MSS time series persisted until December 1994, after which the relative bias was reversed (Figure 1b). Observed monthly differences are often very large, with a difference in the annual totals of up to 507 mm in 2011. These differences and the reversals in biases could be the function of the instrumentations used in the two adjacent sites, as various changes in instrument types have occurred (Table 1). The observed reversal in relative biases coincides with the shift in 1995 to an electronic data-logging system for the PUB instrument. The differences between the PUB and MSS time series from 1990 onwards provide a useful opportunity to characterise for this location an estimate of the background measurement error due to instrumentation. This estimate is used as a baseline to evaluate the skill of our reconstructed historical record: i.e. if the estimate of the error of the reconstructed series is no larger than the differences between two acceptable instrumentations located at the same site then the error falls within an "acceptable measurement error" at that particular location.

Table 2 List of identified historical sources of monthly rainfall observations and the observation location as described in each source.

Period Available	Source	Location(s) of Observation
Nov 1839–Feb 1841	J. S. Travelli (1843), *American Journal Arts and of Science*	Ryan's Hill mission school (H11)
1841–Aug 1845	C. M. Elliot, *Singapore Magnetic Observatory Yearbook*	Singapore Magnetic Observatory (H8)
1862–1866	J. D. Vaughn, *Government Gazette*	River Valley Road (H5)
1864–1886	A. Knight, in Wheatley (1881)	Mount Pleasant, Upper Thompson Road (H7)
1869–1883	Principal Civil Medical Officer (P.C.M.O) of the Medical Department, *Government Gazette* and *The Straits Times*	Goodwood Estate (H1) Pauper's Hospital (Tan Tock Seng) (H2) P & O Coy's Depot (H3) Perseverance Estate (H4) General Hospital (Sepoy Lines) (H6) Convict Prison (H9) Kandang Kerbau (KK) Hospital (H10)

(2) HISTORICAL OBSERVATIONS OF RAINFALL (1839–1883)

Historical rainfall data were compiled from a variety of published sources, such as newspaper reports, journal articles, and government records (Table 2). These observations were made by individuals as well as government bodies and include rainfall measurements (in inches) as well as descriptive accounts of the mean monthly weather.

While rainfall is relatively simple to observe, we know from modern records that large uncertainties exist. It is therefore worthwhile to review how instrumentation evolved in the 19th and 20th centuries. In the mid-1800s, two types of rain gauges, the 'common circular' and the older style 'graduated glass-

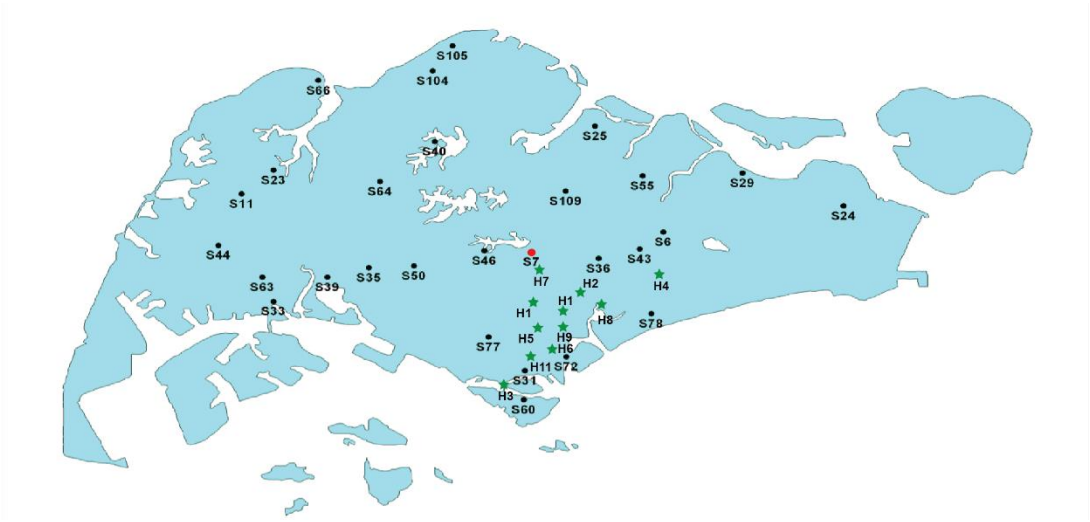

Figure 2 Current 28-station network and identified historical stations. Contemporary AWSs are indicated with black circles and an alpha-numeric code. MacRitchie station (S7) is highlighted in red. Historical stations are indicated by green stars, and tagged as: H1—Goodwood Estate.; H2—Pauper's Hospital; H3—P & O Coy's Depot; H4—Perseverance Estate; H5—River Valley Road; H6—General Hospital; H7—Mount Pleasant; H8—Singapore Magnetic Observatory; H9—Convict Prison; H10—KK Hospital; H11—Ryan's Hill.

measure' type gauges were often used together (BAAS 1855). The new circular gauge was exported from Britain to the colonies by the late 1860s, though standards for using the instrument were not uniformly enforced till the 1880s. During the late 1860s, for example, the rain gauge of Colonial Surgeon H. L. Randall's observational series made at Singapore's Convict Jail was placed 2 ft above the ground, whereas only 1 ft was recommended. Furthermore, many 19th century observational series were made by enthusiastic amateurs (volunteer observational network) rather than trained meteorological staff. These might be plantation owners, such as J. D. Vaughan at River Valley Road, who were given a gauge and some basic, practical advice on how to use it. However, like Vaughan, many of these volunteers had military or naval backgrounds and thus some basic scientific and meteorological understanding. Where observations were made by trained staff, for example at a hospital or a prison, it was under prescribed conditions.

Only quantitative data from published rainfall tables were used in this study, with temporal resolution limited to the monthly scale as few sources provided consistent daily observations. Rainfall tables from the Raffles and Horsburgh Lighthouses, published in the Government Gazette, were excluded from the study on account of their considerable distance from MacRitchie. The compiled historical dataset spans 1839–1883, overlapping with the official MacRitchie meteorological record from 1879–1883 (Table 2, Figure 3). The coordinates of each station had to be determined by cross-comparison of archived historical maps (National Archives of Singapore 2018) with modern-day Singapore geography, since no source provided location data beyond qualitative descriptors (e.g. street/building names). In total, 11 station locations were determined (Figure 2), though with varying accuracy. For example, from 1862—1866, monthly rainfall measurements were taken by J. D. Vaughan and published quarterly in the Government Gazette, with the entire dataset later compiled by Wheatley (1881). Both sources state that the measurements were registered at River Valley Road, providing only a crude location estimate. A map from 1860 places Vaughan's house near the intersection of

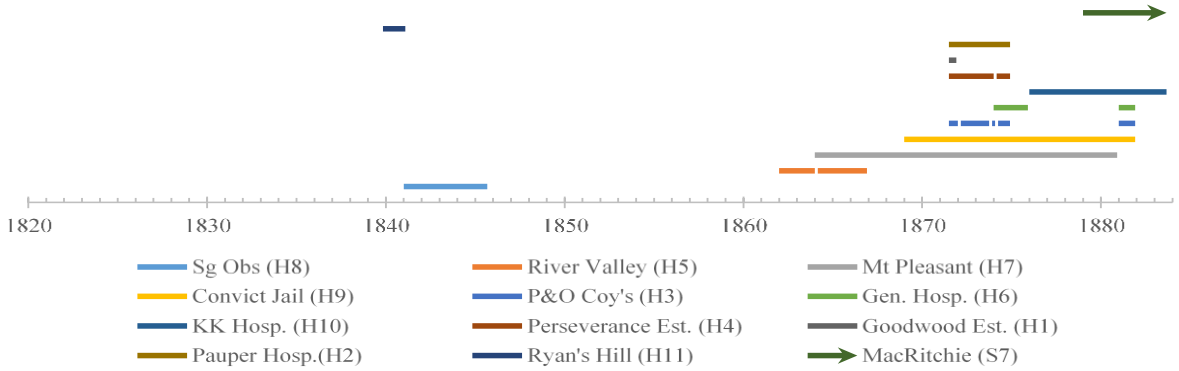

Figure 3 Monthly rainfall data availability for identified historical stations, compared with the current official MacRitchie record (dark green line). Dashed lines highlight the 1879—1883 period used to validate the reconstructed estimated historical MacRitchie series. The shortest station record, Goodwood Estate (dark brown line), is 6 months, whereas the longest station record, Mt Pleasant (grey line), is 204 months (17 years).

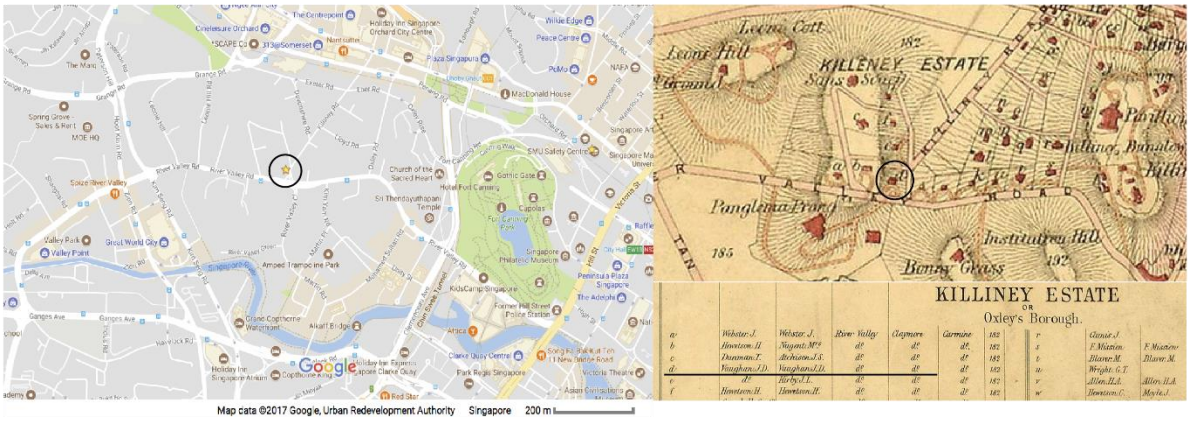

Figure 4 Location of River Valley station, as identified through the map of Killiney Estate from Singapore Residency (1860; National Archives of Singapore 2018). Site of station assumed to be Mr J. D. Vaughan's residence (black circle).

Killiney Road and River Valley Road, which is assumed in this study to be the site of his observations (Figure 4). As rain gauges were not labelled in historical maps (excepting KK Hospital station), stations located in large plantation estates, namely the Perseverance Estate and Goodwood Estate stations, could not be very precisely located. Nevertheless, the impact of location imprecision is likely to be small in comparison with the other uncertainties in this historical reconstruction.

Unfortunately, the historical record is highly fragmented and discontinuous. At present, no data has emerged for the 17-year period between October 1845 and December 1861. In addition, individual station records are relatively short; even the longest station record, Mount Pleasant, is only 17 years long and therefore insufficient on its own to distinguish patterns of decadal variability. Finally, the compiled historical records cannot be directly compared against the contemporary record as none of the identified historical stations are included in the current 28-station meteorological network (Figure 2). Hence, rather than analyse rainfall variability in each individual historical record, the historical data that have been compiled are exploited to attempt to extend the existing MacRitchie record back in time, thereby providing an estimate of historical rainfall for a single site.

METHOD

SPATIAL INTERPOLATION BY INVERSE DISTANCE WEIGHTING (IDW)

In order to reconstruct historical rainfall at MacRitchie station, the spatial relationship of rainfall at the 11 historical stations relative to MacRitchie must be determined. To do so, the spatial pattern is assumed to be stable since the 19th century. The current 28-station network (1980–2014) can be used to approximate the spatial relationship between historical locations in the 19th century. Spatial interpolation by Inverse Distance Weighting (IDW) was chosen as it is fast and easy to implement, enabling new estimates to be rapidly generated whenever revisions to historical station locations are made, or new stations are added:

$$h_{pm} = \frac{\sum_{i=1}^{n}\left(\frac{z_{im}}{d_i^w}\right)}{\sum_{i=1}^{n}\left(\frac{1}{d_i^w}\right)} \quad (1)$$

where h_{pm} is the interpolated rainfall at the location of historical station p for the month m, z_{im} the measured rainfall at contemporary station i for the same month m, d_i the distance between station p and i, and w a positive real number determining the rate of decay in weighting as a function of distance (Shepard 1968). Hence, the monthly rainfall for a historical station is determined by a weighted combination of the set of observed 28-station rainfall for that particular month. As w increases, data from stations further from the interpolated p will have smaller influence (Figure 5). In most geospatial studies, w = 2 is used (e.g. Yang et al. 2015). However, there is no theoretical basis for this number and the optimal value that minimises interpolation error will be heavily dependent on the spatial distribution of known data points (Babak and Deutsch 2008). Here, several values were tested: w = 0.5, 1, 2, 3, 4, and 5. It was found that variations in w had minimal effect on all cross-validation statistics investigated, likely due to the high density of stations across Singapore. In the absence of strong rationale to use a different value, the commonly used value of 2 for w was retained.

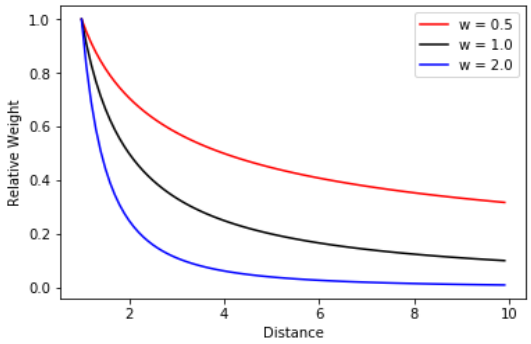

Figure 5 Decay of weighting as a function of distance for various values of *w*.

Another factor affecting the accuracy of IDW is the size of the domain over which stations are selected for interpolation. For this study, we found that limiting the number of stations used (e.g. to the 3 or 6 closest stations) had only a minor effect on mean errors, with accuracy generally improving for higher numbers. However, as missing values are a persistent occurrence across the 28-station rainfall record and to mitigate the effect of missing station data, all 28 contemporary stations were used for the IDW interpolation.

Table 3 Errors associated with IDW interpolation for Kampung Bahru on monthly and annual timescales.

KB' vs *KB* 1980–2014	*r*	MAE	RMSE	MRE
Monthly	0.94	28.9	37.4	0.14
Annual	0.83	127.4	204.9	0.05

The performance of IDW in interpolating station rainfall for Singapore is assessed by recreating the observed monthly rainfall at Kampung Bahru station (S31, Figure 2) from 1980–2014, KB_m, by IDW interpolation using contemporary data from 27 stations

(excluding Kampung Bahru). The hypothetical $KB_{m'}$ is then cross-validated against the actual KB_m using the coefficient of correlation (r), the mean absolute error (MAE), mean relative error (MRE), and root mean squared error (RMSE; Table 3). This station was chosen as it possesses a nearly complete monthly rainfall record, enabling more accurate cross-validation, and is located close to the cluster of identified historical stations. Since IDW is built upon a non-linear distance function, its effectiveness as an interpolator is dependent on the relative geometric distribution of known data points. This effectiveness is unique for each station location but will be similar for stations in close proximity. The comparison between $KB_{m'}$ and KB_m should therefore approximate the effectiveness of IDW in interpolating for rainfall at the locations of the historical stations.

On a monthly scale, the recreated $KB_{m'}$ correlates well with the observed KB_m (Figure 6, Table 3). The calculated r value (0.94) greatly exceeds the threshold for statistical significance ($r_{0.05,n=411}$ = 0.09). Both the MAE (28.9) and RMSE (37.4) are small and on par with the measurement uncertainty reported between the MSS and PUB MacRitchie observations (Table 4), and considering the MRE (0.14), are also relatively minor. The correlation decreases slightly when aggregating the data annually (r = 0.83; $r_{0.05,\ n=30}$ = 0.35), due to the effect of two outliers in 1983 and 2014 where IDW severely underestimated observed annual station rainfall. Nonetheless, on annual scales the MRE is only 0.05, which is in fact smaller than the current MacRitchie instrument error (MRE = 0.09) However, there appears to be a tendency for IDW to slightly underestimate KB_m. From Figure 6, the underestimation seems to stem from inaccurate representation of extreme rainfall events, as errors tend to be significantly larger, and consistently negative, for the wettest months. As IDW is an exact deterministic interpolator, maxima and minima can only occur at known data points. The interpolated point will always be less than the maximum of the set of values used in its calculation (Tomczak 1998). High rainfall months arising from spatially localised convective precipitation centred over Kampung Bahru will thus be consistently underestimated by IDW. Fortunately, systematic errors are mitigated by the density of meteorological stations in Singapore, since the separation between stations are far less than the characteristic length scales of the weather systems affecting Singapore.

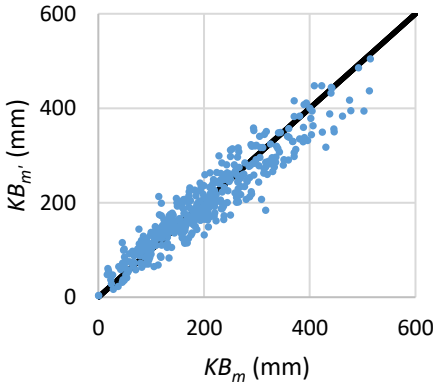

Figure 6 Recreated monthly rainfall at Kampung Bahru for 1980—2014 using IDW spatial interpolation of data from 27-station network ($KB_{m'}$) against actual KB_m. The black line represents a 1:1 relationship.

Reconstructing MacRitchie rainfall from historical station data

IDW spatial interpolation yields 420 rainfall time series data points (monthly values for 1980–2014) for the location of each historical station, which are then compared against the observed monthly MacRitchie rainfall, $MacRF_m$, over the same period. The ratios of $h_{pm}/MacRF_m$ are averaged by month to give $h_{p\bar{m}}/MacRF_{\bar{m}}$. For example, a $h_{p\bar{m}}/MacRF_{\bar{m}}$ value of 1.11 for January for River Valley Road indicates this station received on average 11% more rainfall than MacRitchie station during January for 1980–2014. The historical rainfall measurements compiled for each station, H_{pm}, can then be inverted to give an estimate of historical monthly rainfall at MacRitchie:

$$HMacRF_{pm} = H_{pm} \times \left(h_{p\bar{m}} / MacRF_{\bar{m}}\right)^{-1} \quad (2)$$

where $HMacRF_{pm}$ is the estimate of historical rainfall at MacRitchie by a particular station p for month m. Separate MacRitchie time series are produced from each historical station depending on station data availability, allowing the skill of each individual station reconstruction to be assessed. The final monthly $HMacRF_m$ (1835–1883) compiles all the historical time series, averaging across individual station reconstructions when more than one is available.

Since $MacRF_m$ overlaps with $HMacRF_m$ from 1879 to 1883 (PUB instrument record only), the fit of each historical rainfall reconstruction (Eq. 1, 2) against the observed record can be evaluated using the same validation metrics (r, MAE, MRE, and RMSE). Errors associated with the historical reconstruction are evaluated against the errors registered between the PUB and MSS instruments in the current MacRitchie record. Unfortunately, the relatively short period of overlap only enables the fit of five individual station

$HMacRF_{pm}$ time series to be validated (H3, H6, H7, H9, and H10). Finally, the correlation of each $HMacRF_{pm}$ time series against each other, where there is overlapping data, is also assessed to determine the robustness of the reconstruction technique.

Results and Discussion

The reconstructed historical MacRitchie monthly rainfall time series, $HMacRF_m$, is presented in Figure 7(a). A large gap exists between October 1845 and December 1861, where no published historical data have surfaced yet. Much of the meteorological data collected begins in the late 1860s onwards, giving a continuous rainfall record from Jan 1862–Dec 1883.

Reliability of historical MacRitchie reconstruction

In reconstructing $HMacRF_m$, Eq. 2 assumes that the temporal and spatial relationship of rainfall between stations has not changed as a result of climate change, nor urbanisation factors. Ignoring the effects of urbanisation is highly tenuous, especially considering the rapidity of Singapore's urban development since the 19th century, but is perhaps reasonable in this study as the identified stations were located in historically urban areas, and therefore experienced much less land use change than other parts of Singapore. Indeed, the consistency of station-by-station $HMacRF_p$ (r > 0.8 typically, based on comparisons between stations with overlapping records) supports the long-term stability of spatial relationships.

Cross-validation of the composite $HMacRF_m$ time series against $MacRF_m$ for the period of 1879–1883 suggests that, although errors on a monthly scale are indeed larger than IDW interpolation alone, these errors are relatively small. r (0.81) is still well above thresholds of statistical significance ($r_{0.05,n=60}$ = 0.25), though MAE (43.6) and RMSE (56.7) are slightly larger,

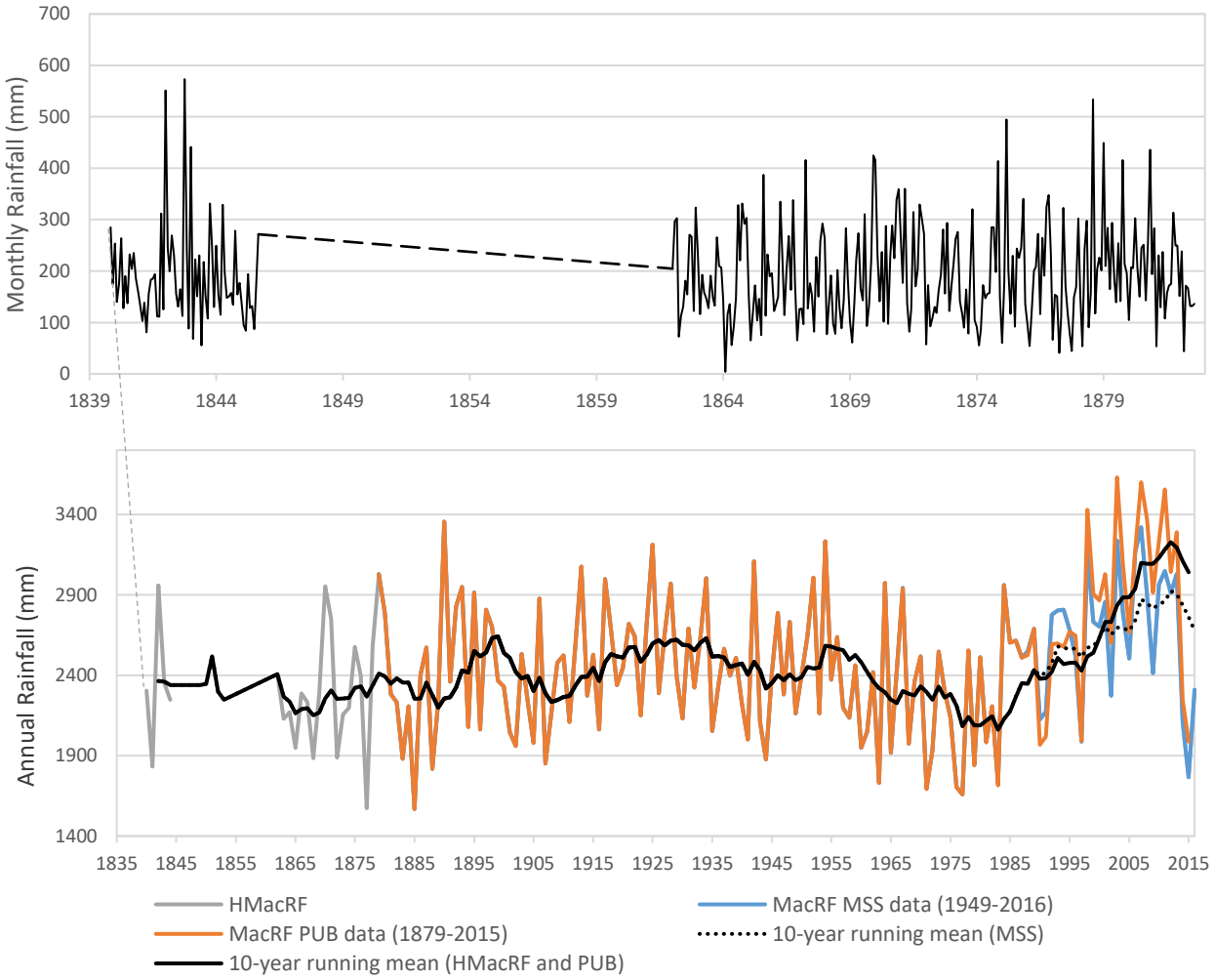

Figure 7 (a) Reconstructed historical MacRitchie monthly rainfall time series ($HMacRF_m$), based on averaging available historical station estimates ($HMacRF_{pm}$) for the period 1835—1883. (b) Annual rainfall time series, including official records, with 10-year running mean.

Table 4 Cross-validation statistics between reconstructed *HMacRF* and official MacRitchie rainfall (*MacRF*) for the period 1879—1883. Statistics for December use individual station estimates. The difference between PUB and MSS records for 1990–2015 are also shown.

	n		r	MAE	RMSE	MRE
$HMacRF_m$ vs. $MacRF_m$ (1879 –1883)						
Monthly	All	60	0.81	43.6	56.7	0.21
	Dec	12	-	94.0	110.7	0.46
3-Monthly	58		0.84	21.2	26.9	0.09
Annual	5		0.97	147.9	165.7	0.06
KK Hospital (H10)	60		0.78	46.6	62.6	0.24
Convict Jail (H9)	36		0.80	49.8	63.8	0.24
Mount Pleasant (H7)	24		0.93	26.1	33.4	0.11
PUB vs MSS (1990–2015)						
Monthly	312		0.99	20.2	26.5	0.09
Annual	26		0.91	233.8	260.3	0.09

giving a MRE of 0.21 (Table 4). Both MAE and RMSE are considerably lower than the mean standard deviation in monthly rainfall observed for $MacRF_m$ from 1980–2014, which ranges between 70.3 mm for June to 149.9 mm for January. There also appears to be no systematic bias in error magnitude as a function of monthly rainfall. Notwithstanding the small sample size, errors associated with annual rainfall estimates are effectively no different from IDW (Table 3) and only slightly larger than the modern instrument error baseline (r = 0.91) with similarly high correlation (r = 0.97; $r_{0.05,n=5}$ = 0.81), and low MAE (147.9), RMSE (165.7) and MRE (0.06). Surprisingly, there is a reduced tendency for underestimation of annual rainfall, which could be the result of averaging estimates, both across stations in building $HMacRF_m$ and within stations in using the mean monthly $h_{p\bar{m}}/MacRF_{p\bar{m}}$.

However, the use of the annual mean $h_{p\bar{m}}/MacRF_{p\bar{m}}$ may underestimate changes in rainfall variability over time, compounding the shortfalls of the IDW interpolation. $h_{p\bar{m}}/MacRF_{p\bar{m}}$ is fairly constant throughout the year and across stations (Table 5), suggesting that seasonal rainfall variability is fairly spatially consistent, with the exception of December, January, and February. For these three months, the standard deviation of calculated ratios over 35 years is substantial, implying significant temporal variability, consistently across all stations. The use of the annual mean $h_{p\bar{m}}/MacRF_{p\bar{m}}$ ratio in the historical reconstruction may thus be unsuitable for DJF season, possibly due to the dominance of the large scale rainfall (e.g. cold surges) characteristic of the early phase of the Northeast Monsoon. Considering the average standard deviation of December $h_{pm}/MacRF_{pm}$ across all stations (1.49), the 95% confidence interval for the December mean ratio is captured by a range of ±0.49, which gives variations in the historical MacRitchie reconstruction of ±50-100 mm. Nevertheless, the average monthly standard deviation for the MacRitchie (PUB) time series (1879–2016) during December is 127.9 mm, so it should be possible to detect signals of natural variability even during the most uncertain month of the year. Smoothing $HMacRF_m$ using a 3-month running mean also reduces errors (Table 4), suggesting the reconstructed time series may be useful for seasonal analyses.

Part of the monthly variability in $h_{p\bar{m}}/MacRF_{p\bar{m}}$ may be mitigated by preferentially selecting/weighting stations nearest to MacRitchie when building the composite $HMacRF_m$ time series. For example, Mount Pleasant, which is the station closest to MacRitchie, has

Table 5 Standard deviation of $h_{pm}/MacRF_{pm}$ by station from IDW interpolation for the period 1980 – 2014.

	Jan	Feb	Mar	Apr	May	Jun	Jul	Aug	Sep	Oct	Nov	Dec
Goodwood (H1)	0.289	0.833	0.155	0.187	0.244	0.240	0.291	0.160	0.225	0.225	0.172	1.298
Pauper's (H2)	0.213	0.890	0.164	0.179	0.233	0.268	0.309	0.167	0.223	0.222	0.177	1.229
P&O's Depot (H3)	0.692	0.389	0.269	0.314	0.337	0.311	0.365	0.286	0.366	0.397	0.293	2.214
Perseverance Est. (H4)	0.195	1.390	0.257	0.227	0.318	0.413	0.341	0.214	0.276	0.290	0.225	1.253
River Valley Rd (H5)	0.440	0.606	0.202	0.245	0.289	0.290	0.357	0.211	0.292	0.282	0.226	1.694
SGH (H6)	0.700	0.379	0.298	0.327	0.373	0.342	0.394	0.304	0.377	0.376	0.303	2.280
Mount Pleasant (H7)	0.114	0.571	0.084	0.089	0.126	0.123	0.145	0.080	0.108	0.113	0.084	0.616
Sg Observatory (H8)	0.221	0.926	0.178	0.193	0.261	0.297	0.356	0.189	0.254	0.255	0.197	1.354
Convict Prison (H9)	0.370	0.670	0.182	0.226	0.277	0.282	0.368	0.201	0.280	0.274	0.218	1.594
KK Hospital (H10)	0.290	0.828	0.160	0.194	0.252	0.260	0.325	0.173	0.243	0.240	0.187	1.384
Ryan's Hill (H11)	0.289	0.833	0.155	0.187	0.244	0.240	0.291	0.160	0.225	0.225	0.172	1.298

the lowest spread of $h_{p\bar{m}}/MacRF_{p\bar{m}}$ ratios in December. Looking at the reconstructed time series from individual stations (Table 4), it is again apparent that errors are smaller closer to MacRitchie, with the stations in Table 5 listed in descending order of distance from MacRitchie, although the amount of data for each station varies. Determining how this weighting function should evolve with distance from MacRitchie requires further study. In the study's absence, the final $HMacRF_m$ time series is built using a simple average of available $HMacRF_{pm}$ data, with station reconstructions given equal weighting regardless of distance to MacRitchie.

CONCLUSION

Singapore is fortunate to have possibly the longest single-site historical monthly rainfall record within the tropics, with the MacRitchie station extending as far back as 1879. However, the reliability of reported rainfall measurements is not without question, with various data sources indicating different values. We have shed new light on the differences between the various data sources to help produce an authoritative time series.

In addition, newly discovered historical source materials provide monthly observations as far back as 1835, albeit incomplete. Through careful review of archived historical map data, the locations of the identified meteorological stations have been determined. By estimating the spatial relationships of rainfall over Singapore using the modern meteorological station network, a reconstructed historical rainfall at the MacRitchie location has been generated, thereby integrating these fragmented historical datasets with the official long-term Singapore rainfall record.

This single time series extended back in time and documented in terms of the difference between various records for the modern area provides a strong basis for studies on decadal to inter-decadal climate variability in Singapore and the neighbouring Western Maritime Continent. Meanwhile, the search for alternative sources of rainfall data during the 1840s to 1860s will continue to help fill in the remaining gaps in the current historical reconstruction.

An important caveat to note for future use of this time series, is that due to uncertainties regarding the variability of spatial rainfall distributions, as well as the precise location of some of the historical measuring stations, analysis of the reconstruction should be limited to seasonal and annual time scales, and relying on single month values should be avoided especially for the winter months (December, January and February).

Further studies, examining the spatial pattern of rainfall in Singapore, could help constrain the parameters used in the IDW interpolation, as well as investigate other interpolators than IDW. This could enable the inclusion of a wider range of historical station data, for example measurements taken at the Raffles and Horsburgh Lighthouses, which could help fill the gaps in the reconstruction.

REFERENCES

Babak, O., Deutsch, C.V. (2008) Statistical approach to inverse distance interpolation. *Stochastic Environment al Research and Risk Assessment*, 23:543–553.

BAAS (1855) Report of the 25th Meeting of the British Association for the Advancement of Science held September 1855, John Murray, London, pp. 30–34.

Marzin, C., Rahmat, R., Berni, D., Bricheno, L., Buonomo, E., Calvert, D., Cannaby, H., Chan, S., Chattopadhyay, M., Cheong, W.K. et al. (2015) Singapore's Second National Climate Change Study – Phase 1. Available at: ccrs.weather.gov.sg/Publications-Second-National-Climate-Change-Study-Science-Reports/, last accessed 18 December 2018.

Nash, D.J., Adamson, G.C.D. (2014) Recent advances in the historical climatology of the tropics and subtropics. *Bulletin of the American Meteorological Society*, 95:131–146.

National Archives of Singapore (2018) Archives online. Available at: www.nas.gov.sg/archivesonline, last accessed 1 December 2018.

Shepard, D. (1968) A two-dimensional interpolation function for irregularly-spaced data. Proceedings of the 1968 ACM National Conference, pp. 517–524.

Tomczak, M. (1998) Spatial interpolation and its uncertainty using automated anisotropic Inverse Distance Weighting (IDW) - cross-validation/jackknife approach. *Journal of Geographic Information and Decision Analysis*, 2:18–30.

Wheatley, J. J. L. (1881) Notes on the rainfall of Singapore. *Journal of the Straits Branch of the Royal Asiatic Society*, 7:31–50.

Yang, X., Xie, X., Liu, D.L., Ji, F., Wang, L. (2015) Spatial Interpolation of Daily Rainfall Data for Local Climate Impact Assessment over Greater Sydney Region. *Advances in Meteorology*, doi:10.1155/2015/563629.

A SEASONAL PERSPECTIVE OF THE MADDEN-JULIAN OSCILLATION'S IMPACT ON SINGAPORE RAINFALL

Cheong Wee Kiong and Zheng Kaiyuan

Central Forecast Office, Weather Services Department, Meteorological Service Singapore

INTRODUCTION

The Madden-Julian Oscillation (MJO) is a source of large-scale atmospheric variability that occurs on an intraseasonal timescale (30–90 days) that is accompanied by deep convection propagating eastwards near the equator. It was discovered in 1971 by Roland Madden and Paul Julian from the National Center for Atmospheric Research after they observed a long-period variation in the surface pressure and zonal winds while analysing measurements made at the Canton Island (Madden and Julian 1971).

Several studies have documented the MJO's influence on the variability of rainfall over the Pacific islands, in the monsoon regions of Asia (Sui and Lau 1992; Lawrence and Webster 2002), and Australia (Hendon and Liebmann 1990). Xavier et al. (2014) showed that convectively active (suppressed) phases of MJO can increase (decrease) the probability of extreme rain events over the land regions of Southeast Asia by about 30–50% (20–25%) during the November–March season.

Singapore has a climate characterised by frequent and intense rainfall, high humidity and high temperature, which are almost constant throughout the year. There are no marked wet and dry periods as rainfall occurs in every month of the year (Figure 1), nevertheless mean monthly rainfall shows drier weather conditions during the Southwest Monsoon (June to September) and wetter conditions in the months of November to January (wet phase of the Northeast Monsoon). During the dry phase of the Northeast Monsoon season (late January to mid-March), it is not uncommon to experience fair and occasionally windy days with little or no rain. However, as the wind-driven weather patterns affecting Singapore are chaotic and with Singapore's small geographical extent, it is challenging to forecast the amount of rainfall over Singapore.

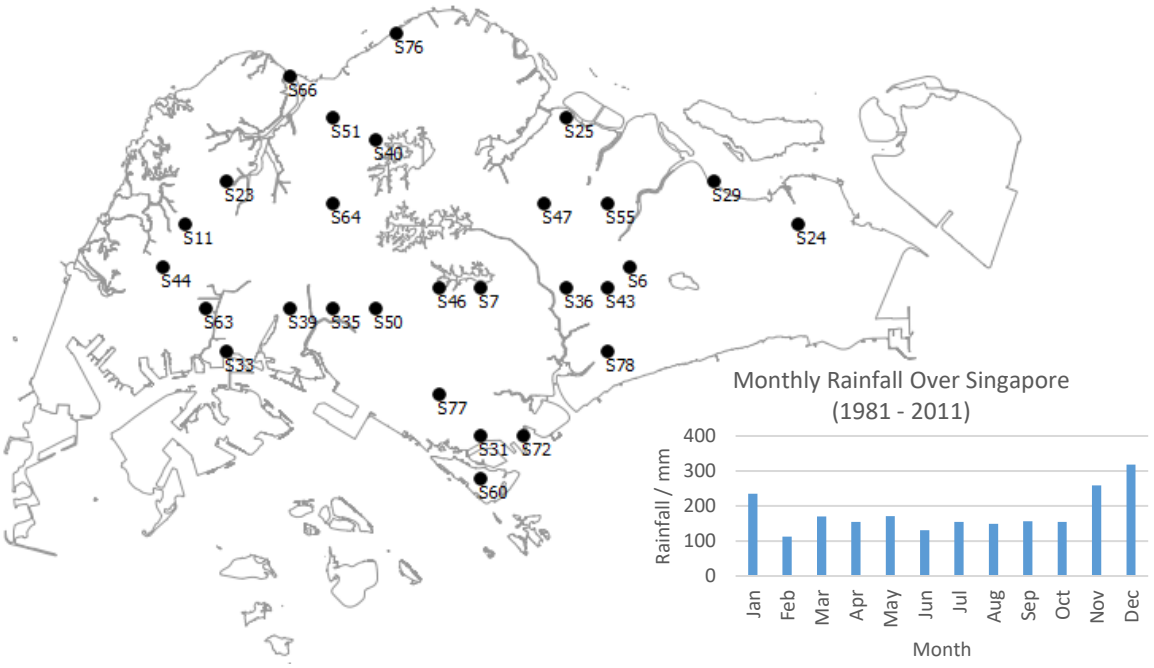

Figure 1 Locations of the 28 rainfall stations used in this study (bottom right numbers indicate the station codes). Maximum of the daily rainfall were extracted from these 28 stations to construct the multi-station daily maximum time series. Bottom right corner of the figure shows the average monthly rainfall over Singapore using climatological rainfall data from 1981–2011.

Singapore is located within the Maritime Continent where the MJO has an effect in modulating the weather patterns, and many of the current numerical weather prediction models show useful skill in forecasting MJO phases 2–3 weeks ahead (Matsueda and Endo 2011). Therefore, it motivates us to investigate and quantify the influences of the MJO on Singapore's rainfall with the objective of providing guidance in forecasting rainfall amount over Singapore using predicted MJO conditions.

DATA AND METHOD

Meteorological Service Singapore has since 1980 recorded hourly rainfall data across an island-wide network of 28 real-time automatic weather stations using tilting-siphon rain recorders. The distribution of stations over the island is shown in Figure 1. For this study, data from 1980 to 2011 were used. From these data, a multiple-station daily time series is computed by extracting the maximum of the daily rainfall from all the 28 stations. The rationale for using the maximum rainfall rather than the average rainfall across the 28 stations was to provide guidance in forecasting extreme rainfall, which is valuable to operational weather forecasters.

The dataset has been quality controlled using basic procedures (e.g. negative daily precipitation amounts were removed). Only two stations have incomplete instrumental records: S72 (Tanjong Pagar), available from 1982 to 2011 and S76 (Admiralty West), from 1982 to 2009. All time series contain less than 10% of missing data. In order to capture the annual cycle, the rainfall data is clustered into 2-month bins. From the daily pan-island rainfall time series, several statistics were computed: percentage of rain days (days with rainfall intensity ≥ 1mm), as well as median and percentiles of daily rainfall intensity for each of the 2-month clusters.

To investigate the seasonal dependency on the impacts of the MJO on Singapore rainfall, the commonly used all-season Real-time Multivariate MJO (RMM) Index was used, based on Wheeler and Hendon (2004) and is available on the Australian Bureau of Meteorology website (BoM 2018).

MJO episodes were qualified as either strong (RMM amplitude > 1) and weak (RMM amplitude ≤ 1) and counted for each 2-month clusters (Figure 2). On average there are more strong than weak MJO days—out of the total number of cases in the dataset, 59.6% are strong MJO days while 40.4% are weak MJO days. In addition, strong MJO days occur around 62% of the time in the Northeast and inter-monsoon months (October to May) and 55% of the time in the Southwest Monsoon months (June to September). Generally, the data are relatively well distributed across the 2-month clusters except for fewer cases in Phases 1 and 2 of strong (RMM amplitude >1) MJO episodes during February to March (Figure 2b) and in Phase 7 during August to September (Figure 2e).

The rainfall statistics were then differentiated for the various 2-month clusters based on the MJO phases and magnitude. A difference is considered to be statistically significant if significant at the 5%-level using the binomial p-value test with reference to the sample in each individual cluster. Overall the difference in sample sizes across the clusters is limited and the sample size for each cluster is large enough to ensure robust results and do not impact the analyses proposed.

RESULTS AND DISCUSSION

Before looking at rainfall amount, the role of the MJO on the frequency of occurrences of rainfall is investigated. The percentage of raindays (not shown) indicates no significant differences in all phases of the MJO activity for the annual mean, as well as for the 2-month clusters, except during Phase 6 of both strong and weak MJO episodes. However, a lower percentage of raindays are noted during the Southwest Monsoon: a decrease from 79% for all phases to 63% and 68% for June–July and August–September, respectively.

To assess the impact of MJO on rainfall amount, the median daily rainfall totals are evaluated during strong and weak MJO episodes. The term "moderate raindays" is used for days with daily rainfall totals higher than the median daily rainfall totals recorded over all MJO phases. This is shown for the annual mean and for the six 2-month clusters (Figure 3).

During strong MJO episodes, Singapore experienced higher median rainfall amounts during Phases 1-4 and lower amounts during Phases 5-7 almost throughout the year (Figure 3a). Nearly half of the 2-month statistics indicate a significant tendency. A higher percentage of moderate raindays was experienced during Phase 3 of strong MJO episodes when intense organised convection occurs over the western Maritime Continent in the Northeast Monsoon and inter-monsoon months from October to May (Figure 3g, b-d). For the Southwest Monsoon season, statistically significant higher percentage of moderate raindays are observed during Phase 2, instead of Phase 3, of the strong MJO episodes i.e. when intense organised convection occurs over the East Indian Ocean (Figure

3e, f). The northward propagation and variability of the MJO extending further from the equator during boreal summer, compared to the eastward propagation around the equator during the boreal winter, could be contributing towards the differences across seasons (Kemball-Cook and Wang 2001).

Another interesting result is the statistically significant higher percentage of moderate raindays during the inter-monsoon months (April–May and October–November) when strong MJO activity is over the West Indian Ocean (Phase 1), which is relatively far from Singapore (Figure 3d, g). Such tendency in higher percentage of moderate raindays during this period of time could most probably be attributed to locally develop intense thunderstorms, and not necessarily directly influenced by the MJO. During these inter-monsoon months, the sun is almost directly overhead at the equator, and locally developed intense thunderstorms mainly caused by strong convection due to strong solar heating of land areas are common over Singapore.

When deep organised convection occurs over the Central Pacific Ocean (strong MJO in Phase 6), a generally lower percentage of moderate raindays is experienced throughout the year, except in February–March when no significant tendency is observed in the statistics (Figure 3). During December–May and June–November, Singapore experiences a lower percentage of moderate raindays when deep organised convection occurred over the western and eastern Pacific Ocean (strong MJO in Phases 5 and 7) respectively (Figure 3). It is also notable the significant decrease in the median of

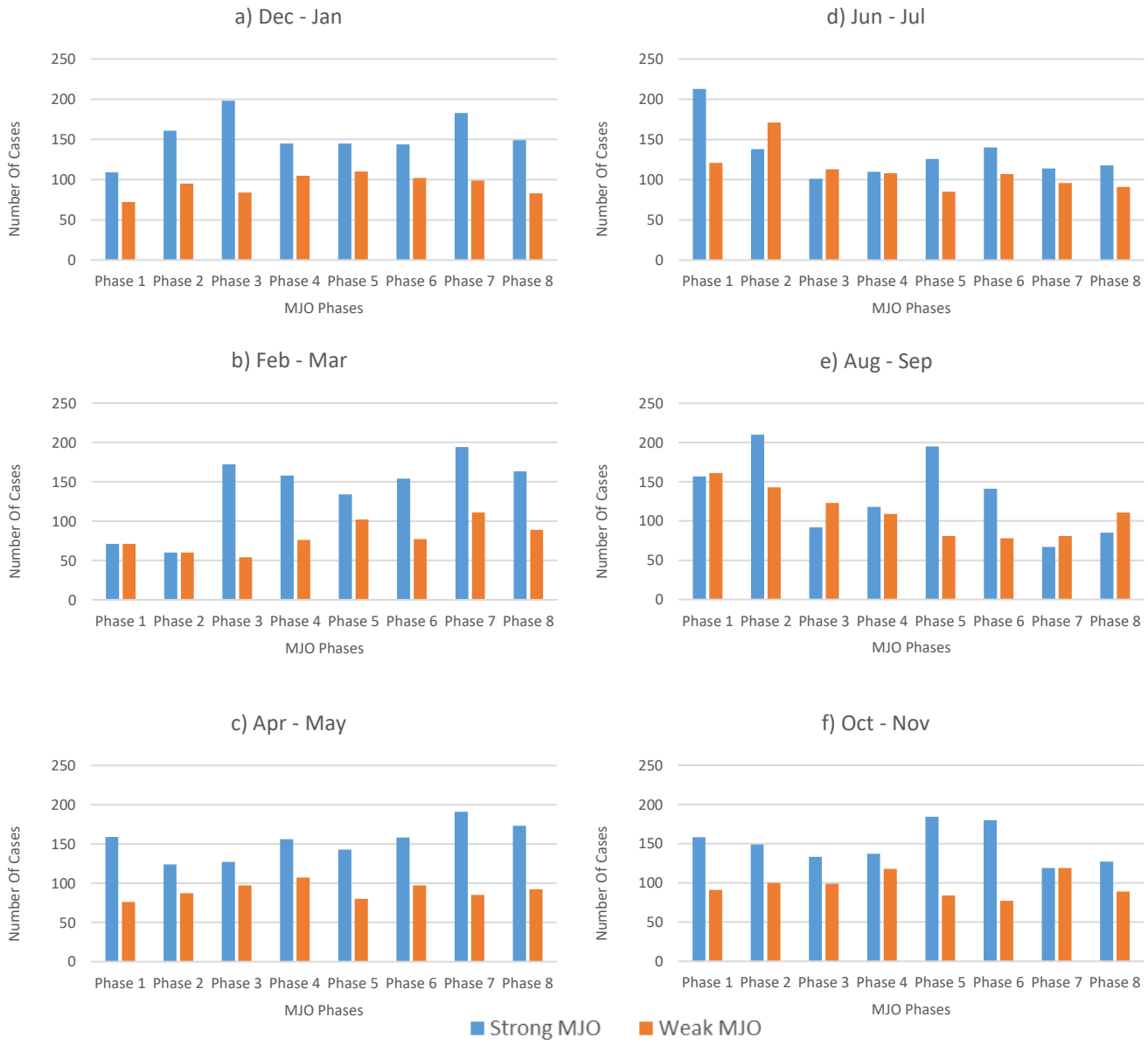

Figure 2 Bi-monthly number of cases considered for strong MJO (RMM amplitude > 1, blue) and weak MJO (RMM amplitude ≤ 1, orange) across all MJO phases between 1980–2011.

the daily rainfall intensity during the Southwest Monsoon (June – September) when strong MJO is in Phase 6 (Figure 3d, e, f).

During weak MJO (amplitude < 1) episodes, there is generally no significant impact on the percentage of moderate raindays over Singapore, except for the few instances highlighted in Figure 3.

For very heavy raindays (defined as days with daily rainfall totals ≥ 70mm, the 90th percentile) over Singapore, MJO activity has an influence on the

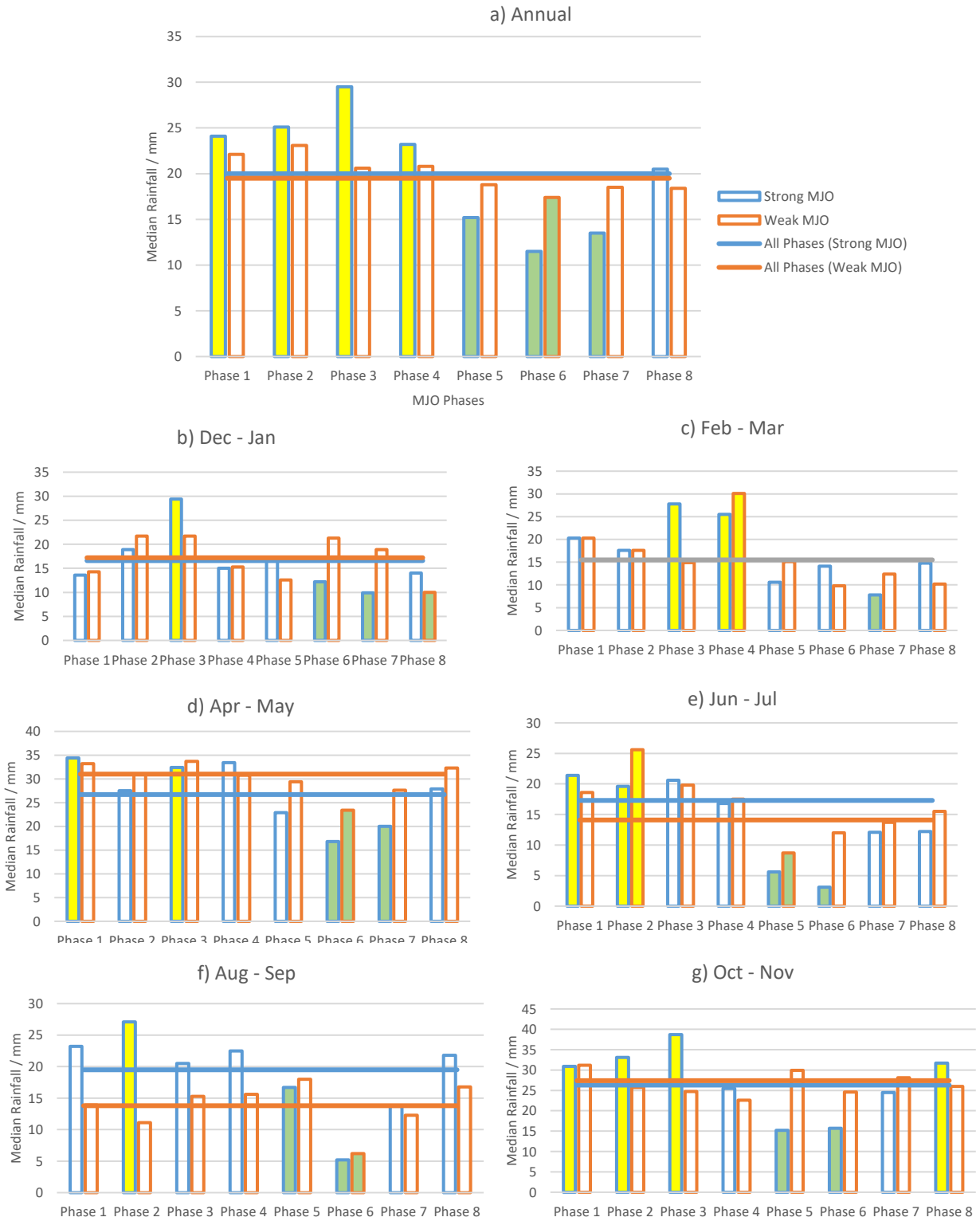

Figure 3 Median daily rainfall totals (mm). Height of bars indicates the median rainfall totals for each MJO phase and the border colour indicates the strength of MJO (blue – strong and orange – weak). Horizontal line indicates the median rainfall regardless of the MJO phases and colour indicates the strength of MJO. Yellow/green shaded areas indicate statistically significant (at 5% level) higher/lower percentage of days with daily rainfall intensity heavier than the median of the daily rainfall totals recorded over all MJOs' phases.

percentage of days, in particular in Phases 3, 6, and 7. When strong MJO is in Phase 3, a tendency to a higher percentage of very heavy raindays is observed during October– January and April–May (18.1% of the time, relative to the average frequency of 12.4%; Figure 4b, d, g). This relationship is similar to that for the percentage of moderate raindays. The statistically significant tendency in a higher percentage of moderate raindays during February–March however, is not detected for the percentage of very heavy raindays (Figure 4c). Interestingly, a higher percentage of very heavy raindays during October–March is experienced when weak MJO is observed over the East Indian Ocean (Phase 2; Figure 4b, c, g); this relationship is not observed for the percentage of moderate raindays discussed above.

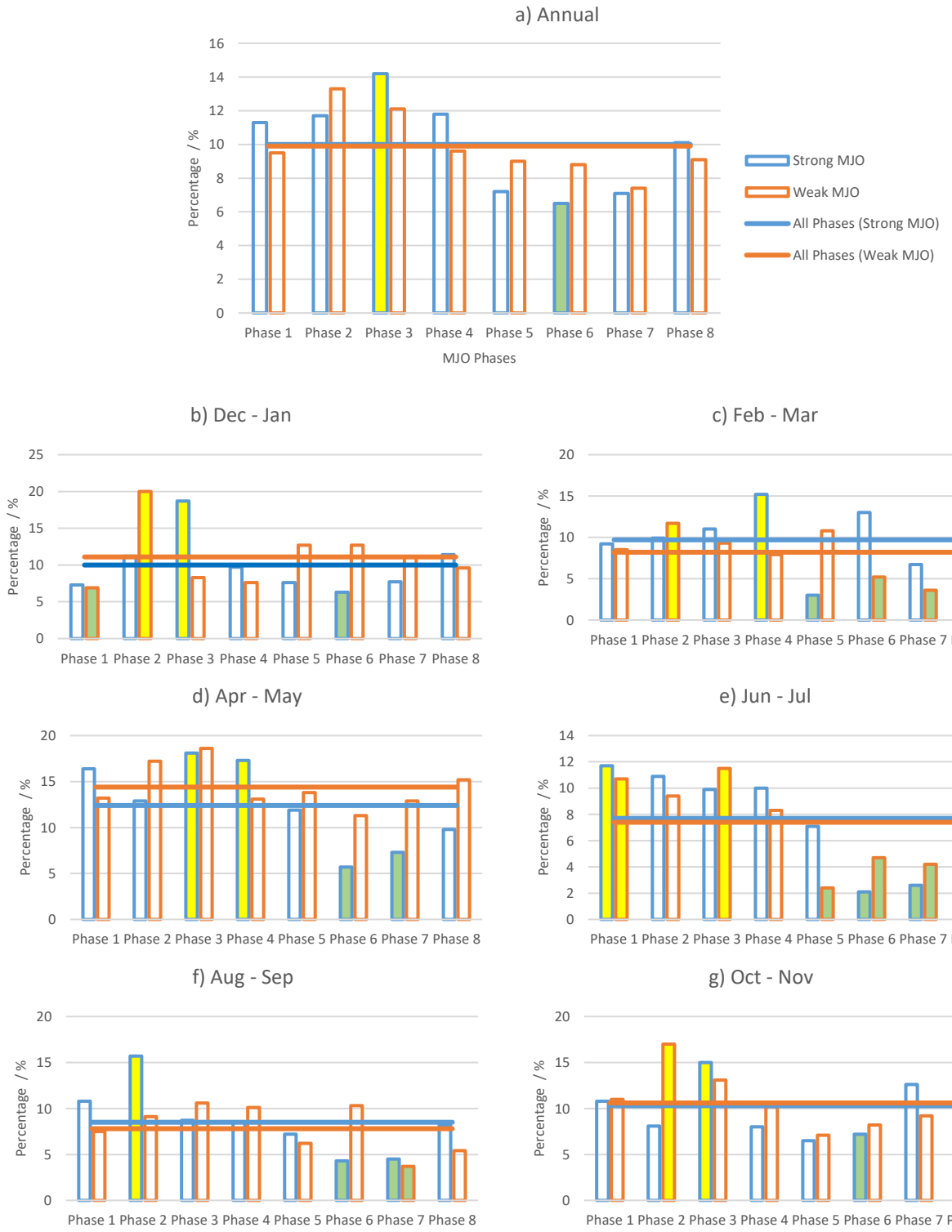

Figure 4 Same as Figure 3, but for percentage of days with daily rainfall totals above 70mm (very heavy raindays). Units are in %.

A statistically significant lower percentage of very heavy raindays are noted during April–September, when deep organized convections occurred over the Central Pacific Ocean and East Pacific Ocean (Phases 6 and 7) respectively (Figure 4d-f).

CONCLUSION

This study presents evidence that the MJO phases and amplitude modulate the daily rainfall intensities over Singapore. In general, Singapore experiences a higher percentage of moderate and very heavy raindays when strong MJO activity occurs over the western Maritime Continent (Phase 3) during the Northeast Monsoon and inter-monsoon months (October–May) while a higher percentage of heavy raindays are observed when strong MJO activity occurs over the East Indian Ocean (Phase 2) during the Southwest Monsoon months (June–September). In general, a lower percentage of moderate and very heavy raindays are experienced when deep organized convection occurs over the Central Pacific Ocean (strong MJO in Phase 6). The impact on the rainfall over Singapore during weak MJO (amplitude < 1) episodes is relatively limited and isolated, except for the higher percentage of very heavy raindays persisting from October to March when weak MJO occurs over the East Indian Ocean (Phase 2). This highlights that more than one aspect of weather statistics is required when investigating the relationships between local rainfall and large-scale weather phenomena, as different weather statistics might lead to different conclusions. While some local rainfall statistics may not exhibit strong relationships with large scale phenomenon, other local rainfall statistics may indicate otherwise.

The present study shows that while the MJO has minimal impact on the frequency of raindays, it strongly modulates the rainfall intensities over Singapore. While other drivers besides MJO activity are also likely to impact rainfall statistics, the results presented here provide useful guidance for forecasting at the subseasonal-to-seasonal timescale.

REFERENCES

BoM (2018) Realtime MJO index. Available at: www.cawcr.gov.au/staff/mwheeler/maproom/RMM/RMM1RMM2.74toRealtime.txt, last accessed: 5 October 2018.

Hendon, H. H., Liebmann, B. (1990) The intra-seasonal (30-50 day) oscillation of the Australian summer monsoon. *Journal of Atmospheric Science*, 47:2909–2923.

Kemball-Cook, S., Wang, B. (2001) Equatorial waves and air–sea interaction in the boreal summer intraseasonal oscillation. *Journal of Climate*, 14:2923-2942.

Lawrence, D.M., Webster, P.J. (2002) The boreal summer intra-seasonal oscillation: Relationship between northward and eastward movement of convection. *Journal of Atmospheric Science*, 59:1593–1606.

Madden, R. A., Julian, P. R. (1971) Detection of a 40–50 day oscillation in the zonal wind in the tropical Pacific. *Journal of Atmospheric Science*, 28:702–708.

Matsueda, M., Endo H. (2011) Verification of medium-range MJO forecasts with TIGGE. *Geophysical Research Letters*, 38: L11801.

Sui, C.H., Lau K.M. (1992) Multiscale phenomena in the tropical atmosphere over the western Pacific. *Monthly Weather Review,* 120:407–430.

Wheeler, M. C., Hendon, H. H. (2004) An all-season real-time multivariate MJO index: Development of an index for monitoring and prediction. *Monthly Weather Review*, 132:1917–1932.

Xavier, P., Rahmat, R., Cheong, W.K., Wallace, E. (2014) Influence of Madden-Julian Oscillation on Southeast Asia rainfall extremes: Observations and predictability. *Geophysical Research Letters*, 41:4406–4412.

SUBSEASONAL FORECASTING OF MAJOR WET SPELLS IN THE SOUTHERN MALAY PENINSULA

Sharmaine Toh Xiao Min[1], Thea Turkington[2], Mou Leong Tan[3], Raizan Rahmat[2]

[1]Department of Geography, National University of Singapore, [2]Subseasonal and Seasonal Prediction Section, Centre for Climate Research Singapore, [3]Geography Section, School of Humanities, Universiti Sains Malaysia

INTRODUCTION

Flooding is one of the main hydro-meteorological hazards for the southern Malay Peninsula (Tan et al. 2018). For example, the December 2006 to January 2007 floods were one of the worst floods in the region causing at least 17 deaths, 103,000 residents to be displaced, 800 badly damaged or destroyed houses, and an estimated 52,000 hectares of damaged agricultural land (DREF 2007). To help prepare for and mitigate such events, weather and seasonal climate predictions are used.

Given the timescales over which flood events occur, subseasonal-to-seasonal (S2S) forecasts have the potential to be useful. An S2S forecast database has been available since 2015 as part of the WWRP/WCRP S2S Prediction Project (Vitart et al. 2017). These forecasts, submitted by several operational centres, provide meteorological information for two weeks to two months into the future: providing a longer lead time than traditional weather forecasts of a couple days and more detailed information than seasonal forecasts. These two factors are important for extreme events. It has already been shown that the overall skill of S2S models in predicting precipitation is relatively high for Southeast Asia (Li and Robertson 2015). However, there have been few case studies analysing model performance for extreme hydro-meteorological events for this region.

This letter analyses S2S forecasts for selected extreme hydro-meteorological case studies over the southern Malay Peninsula, in particular for the Johor River Basin (JRB). The S2S forecasts are assessed along with the background meteorological conditions, such as the Madden Julian Oscillation (MJO) and Northeast Monsoon cold surges. The evaluation of the case studies is also compared to overall skill of the model.

STUDY AREA

Johor River Basin lies between latitudes 1.5°N and 2.2°N, and longitudes 103°E and 104°E (Tan et al. 2018). The length of the Johor River is about 122 km and flows in a north–south direction towards the Straits of Johor (Figure 1). The catchment spans a total area of about 1652 km^2 with elevation ranging between 3 m and 977 m above mean sea level (Tan et al. 2018). Flooding is the main hydro-meteorological hazard in JRB and occurs frequently during the Northeast Monsoon between the months of December to March (Tan et al. 2015).

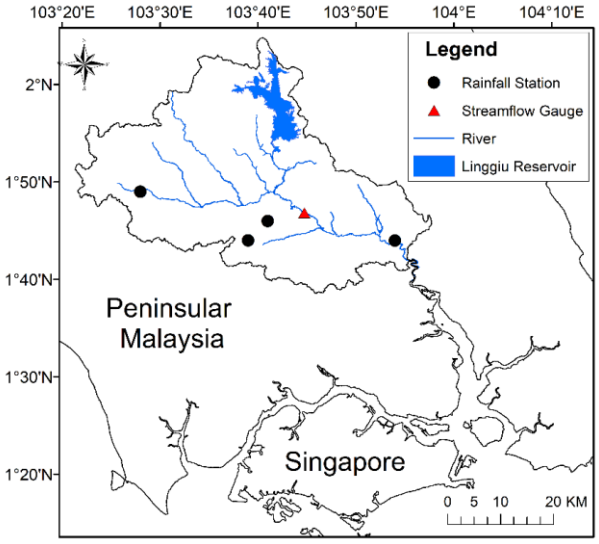

Figure 1 Map of Johor River Basin, including Rantau Panjang streamflow gauge (red triangle).

The region's climate is influenced by drivers at various spatial scales. Large-scale atmospheric drivers include those such as El Niño–Southern Oscillation (ENSO) and the Indian Ocean Dipole. The MJO, one of the main subseasonal drivers globally, tends to bring more rainfall during Phases 2–4 and drier conditions during Phases 6–8 for the region (Xavier et al. 2014). During the Northeast Monsoon, strong winds over the South China Sea associated with southward intrusions of the Siberian high bring increased convection over the Maritime Continent, termed cold surges (Lim et al. 2017). When cold surges and the MJO occur at the same time, the rainfall pattern tends to more closely resemble a cold surge, with the MJO increasing the extreme rainfall response in the region in Phases 2–4 (Lim et al. 2017).

DATA AND METHODOLOGY

Four case studies were identified based on media reports on flood damages in southern Malay Peninsula (Table 2). Each event was given a seven-day range, a common period used in S2S forecasts, corresponding to the week with the highest rainfall amount either just before or during the flood events.

This study used S2S forecasts from the ECMWF model (Vitart et al. 2017), as this model has shown relatively higher skill than other models for Southeast Asia (Li and Robertson 2015). The model is run every Monday and Thursday, producing 51 ensemble member forecasts up to 46 days in the future. Twenty years of re-forecasts are also produced starting on the same day of the year as the forecast, each comprised of 11 ensemble members. Re-forecasts are similar to forecasts, but run for past dates. These re-forecasts are used for assessing the model's skill and calibrating the model against its climatology. Re-forecasts can also be used for analysing case studies using a newer version of the model. Since S2S ECMWF forecasts are only archived from 2015 onwards, this letter focused on re-forecasts.

Table 1 Summary of data retrieved from IRI Data Library. The original resolution of the ECMWF model varies between 0.25° and 0.50° (Vitart et al. 2017).

	Spatial resolution	Temporal resolution	Temporal coverage
ECMWF (re-forecasts)	1.50°	Daily	1995–2017
CHIRPS	0.25°	Daily	1981–2018
TRMM	0.25°	Daily	1998–May 2015

Two gridded, satellite-based datasets were used for verifying the forecasts: Climate Hazards Group InfraRed Precipitation with Stations (CHIRPS), and Tropical Rainfall Measuring Mission (TRMM). Developed by the US Geological Survey and the University of California, Santa Barbara, CHIRPS is a near-global rainfall dataset. The dataset uses satellite imagery, calibrated by TRMM Multi-Satellite Precipitation Analysis version 7, along with station-based rainfall data to create a gridded rainfall dataset over land (Funk et al. 2015). The other gridded dataset, TRMM, is based on a variety of sensors and sources, such as the TRMM Precipitation Radar for its outputs, and covers both the land and ocean (Huffman et al. 2007). A summary of the resolution and temporal coverage for these two datasets, as well as the S2S ECMWF model, can be found in Table 1. Satellites provide area-averaged rainfall estimates, which contain uncertainties related to the spatial and temporal resolution of the satellites, as well as to the methods used to derive the estimates (Huffman et al. 2007). Therefore, while these datasets are not independent, it is still useful to compare model assessments using different observational datasets.

Weekly re-forecast anomaly plots were created for four lead times for each of the case studies. Lead time 1 refers to the forecast from the start of the first week (the first seven days of the re-forecast), lead time 2 refers to the forecast run starting from a week prior (days 7 to 14 of the re-forecasts), up to lead time 4 that refers to the forecast run three weeks prior to the start of the case study (days 21 to 28 of the forecast). The anomalies were calculated using:

$$a = r - \bar{r} \quad (1)$$

where a is the weekly anomaly, r is the weekly rainfall total and $\bar{r}$ is the average weekly total (1998–2014). In the case of the re-forecasts, the 11 ensemble members were first averaged before calculating the weekly anomalies and climatologies.

The weekly re-forecast anomaly plots were then compared with observed weekly anomaly plots to determine forecast quality. For easier comparison, the TRMM and CHIRPS datasets were re-gridded from the original 0.25° resolution to the 1.50° resolution of the models in the S2S Project database.

To assess the overall skill, the correlation of anomalies (CORA) and mean square skill score (MSSS) were also calculated. CORA, also called "anomaly correlation coefficient", measures the linear association between the predicted anomalies and the observations. Therefore, it measures the relative association between the variables, rather than the overall accuracy of the forecast. CORA varies between 1 (perfect association) and -1, and can be measured using the following:

$$CORA = \frac{\sum(a_{re})(a_{ob})}{\sqrt{(\sum {a_{re}}^2)(\sum {a_{ob}}^2)}} \quad (2)$$

where a_{re} is the reforecast ensemble mean anomaly and a_{ob} is the observed anomaly.

The mean square skill score is based on the mean square error, where the maximum value is 1 for a perfect forecast, and a negative value implies the re-forecast is less skill full than the climatology. When using anomaly values, the MSSS is calculated using:

$$MSSS = 1 - \frac{\sum(a_{re} - a_{ob})^2}{\sum {a_{ob}}^2} \quad (3)$$

For both skill scores, the observed anomaly is based on the TRMM data. CHIRPS was not used as it only

covers land points, and therefore would not provide information for the skill over the ocean. Each month was also calculated independently due to potential seasonal differences in skill.

The IRI Data Library (IDL) was used to retrieve, process, and plot the data (Blumenthal et al. 2014). The IDL is an online data repository and analysis tool using the INGRID Data Analysis Language. The analysis tool allows for easy re-gridding, as well as creating and plotting of anomalies.

Results and Discussion

Four major weather events during the months of December to March were identified. The events are summarised in Table 2, along with the observed average daily rainfall and daily average 925 hPa wind for the mid-point of the week for the events in Figure 2. Cold surges based on Lim et al. (2017) were identified when wind at 850 hPa, averaged over 5°–10°N and 107°–115°E, was greater than 0.75 standard deviations above the mean, while the mean sea level pressure, averaged over 18–22°N and 105–122°E, was greater than 1020 hPa. The ENSO state was based on the Nino 3.4 index (Turkington et al. 2018), while the MJO Phase was based on the RMM index (BoM 2018). A brief description of each event is provided below.

Case Studies

1. *23–29 January 2004*

During this event, the MJO was in the wet phases for the region, continuing the strong MJO activity that developed in December 2003. MJO Phase 2 is associated with active convection over the western Maritime Continent (Lim et al. 2017) and may be why there is less above-average rainfall over the eastern Maritime Continent (top two rows, first column, Figure 3). A cold surge was also present for the first half of the event, noted by the strong north-easterlies in the South China Sea (Figure 2a). The observed rainfall anomaly maps for this event strongly resembles a cold surge, with positive rainfall anomalies over southern Malay Peninsula, as well as western and northern Borneo (Lim et al. 2017).

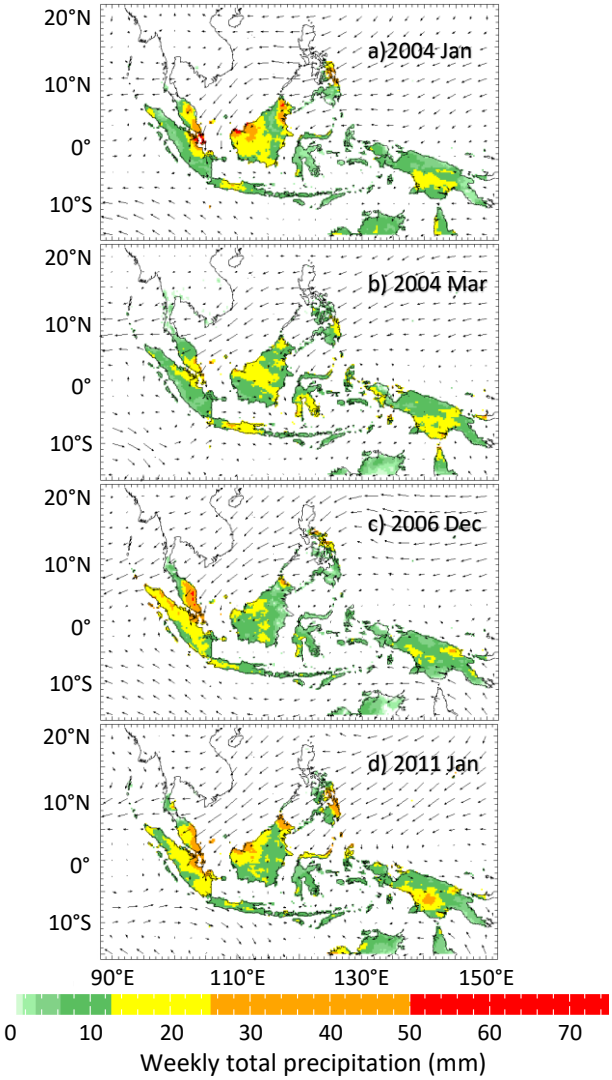

Figure 2 Average daily precipitation during the event week (CHIRPS), and the daily wind direction and speed mid-week (NCEP-NCAR Reanalysis, Kalnay et al. 1996).

Table 2 The four case studies, with associated ENSO states, MJO Phases, and cold surges. As estimates for the size of the events, the weekly average discharge at Rantau Panjang station (Discharge) is provided along with the weekly total measured by the rain gauges (Figure 1) and the CHIRPS and TRMM data (averaged over 1.50°–2.25°N, 103.00°–104.00°E).

	Week	Discharge (m^3/s)	Weekly Total (mm)			ENSO state	MJO Phase	Cold Surges
			Rain Gauge	CHIRPS	TRMM			
1	23–29 Jan 2004	29	225	250	230	Neutral	2–3	22–26 Jan
2	6–12 Mar 2004	108	440	140	230	Neutral	3–4	06–09 Mar
3	16–22 Dec 2006	185	560	260	480	Neutral	3	17–23 Dec
4	25–31 Jan 2011	92	360	250	360	La Niña	8–decay	24 Jan–2 Feb

Even with the smallest recorded discharge in Table 2, homes were evacuated in the region, as well as in Sarawak where 2000 homes were submerged and in Sibu where RM20 million in damages was recorded (Dartmouth 2018a). The entire flood event lasted from 24th January to the 3rd of February.

2. 06–12 March 2004

The MJO Phase for this event was from a wet phase (3) to transitional phase for the region (4). These phases bring above-average rainfall for the entire Maritime Continent (Xavier et al. 2014), similar to the widespread above-average rainfall during this event (top two rows, second column, Figure 3). A cold surge was also present, although the north-easterlies were slightly weaker than the other case studies (Figure 2). Cold surges are less common in March compared to December and January, and those that occur from February onwards tend to bring less rainfall for southern Malay Peninsula (Lim et al. 2017). However, heavy rainfall was still recorded (Table 2, Figure 2b) and could be attributed to the MJO's presence.

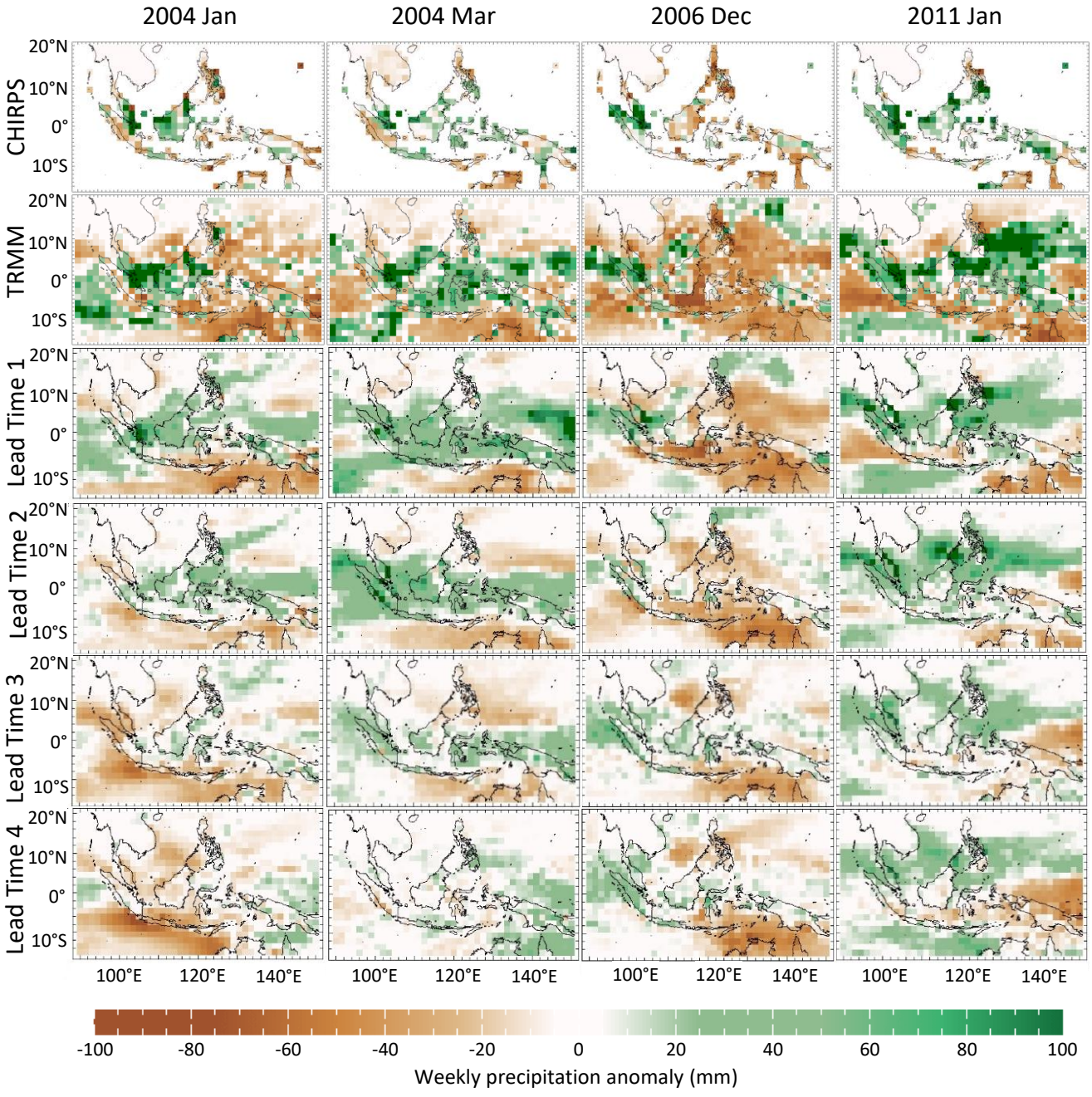

Figure 3 Weekly rainfall anomalies for the 2004 Jan, 2004 Mar, 2006 Dec, and 2011 Jan events. The top two panels show observed anomalies using CHIRPS and TRMM; the lower panels show the re-forecast anomalies from ECMWF at various lead times.

This event recorded the second largest discharge (Table 2), affecting both Singapore and Johor. For Johor 12,400 people were displaced over eight districts in the region (Dartmouth 2018a). The entire flood event lasted from 8th to 13th of March, the shortest of the four case studies.

3. 16–22 December 2006

For this event, a coherent MJO signal only developed in mid-December in Phase 3, as the supressed convection phase of the MJO gradually moved eastward and reaching the Maritime Continent by the end of the case study week. This MJO development may explain why the above-average rainfall is less extensive than for the previous two case studies (first two rows, Figure 3). However, the north-easterlies in the South China Sea associated with an extended cold surge that lasted for six days, contributed to the enhanced rainfall over southern Malay Peninsula.

Recording the largest discharge amount of the case studies, this event also caused significant damage to the region and Singapore. While the heaviest rainfall fell 16th–22nd December, the flood event itself lasted until the 13th of January. More than 90,000 people were displaced in Johor and Malacca, with damages from floods and landslides amounting to 22 million USD (Dartmouth 2018b).

4. 25–31 January 2011

The MJO signal had been in the dry phase prior to the event (Phases 6 and 7 from mid-January). By the 25th of January the MJO was in Phase 8, which normally brings drier conditions, although the MJO decayed rapidly during the week. However, there were strong north-easterlies at 925 hPa (Figure 2d), indicative of a cold surge. Therefore, it is likely the cold surge, which lasted throughout the week, dominated over the MJO. Furthermore, this case occurred during a La Niña event. La Niñas bring above-average rainfall to much of the Maritime Continent, although not necessarily to southern Malay Peninsula, and therefore may explain the wide spread above-average rainfall compared to cases 1 and 3 (top two rows, Figure 3).

The January 2011 flood lasted from the 29th of January to 4th of February, where riverbank overflow affected areas like Segamat, Batu Pahat, Kluang and Muar, resulting in multiple deaths and 24,000 people displaced (Reliefweb 2018).

S2S FORECASTS

The anomaly patterns over Southeast Asia for lead times 1 and 2 (rows 3 and 4, Figure 3) match the TRMM and CHIRPS data (rows 1 and 2, Figure 3) for all case studies. Furthermore, all ensemble mean re-forecasts predict above-average rainfall for southern Malay Peninsula. Regionally, the re-forecasts also pick up the variation between the events, with a smaller extent for the December 2006 case study compared to the other three case studies. Based on these results, a two week lead time shows potential for the prediction of extreme hydro-meteorological events.

The ability of the re-forecasts to capture the heavy rainfall is less consistent between case studies at lead times 3 to 4, most notably for the January 2004 case (rows 5 and 6, Figure 3). The re-forecasts predict drier conditions at these lead times for this case. From the observations however, the pattern resembles a cold surge, suggesting that this is the dominant driver for the event. Cold surges can be tied to mid-latitude weather systems such as the Siberian High. S2S forecast skill is much lower over the mid-latitudes (Li and Robertson 2015), and this link with mid-latitudes may be the reason some events were not predicted at longer lead times. Although, the results from other case studies suggest that some cold-surge events may be predicted at lead times 3 and 4.

For the March 2004 case, the widespread rainfall anomaly is still captured in lead time 3, along with intensified rainfall over southern Malay Peninsula. Even though wet cold surges are unusual for this time of year, the ensemble mean appears to identify this event with a lead time of three weeks, potentially linked with the developing strong MJO at that time. For this case; however, the rainfall anomaly pattern at lead time 4 bears little resemblance to the observed pattern.

For the other two cases, above-average rainfall is forecasted at lead time 3, although the anomaly is not as large as what was observed (row five, Figure 3). At lead time 4, the rainfall anomaly pattern resembles the observed pattern although there are noticeable differences in location, along with weaker anomalies.

SKILL SCORES

Skill scores for December and March were computed using CORA and MSSS to estimate the overall skill of the S2S forecasts for these two months. The scores for the two months are similar (Figure 4), with the band of highest skill following the Intertropical Convergence Zone.

The skill declines from lead time 1 to lead time 4, similar to the case studies. The skill scores are highest for lead time 1. At lead time 2, the scores are higher in CORA than MSSS, although this may be due to CORA being based on only the association, rather than the

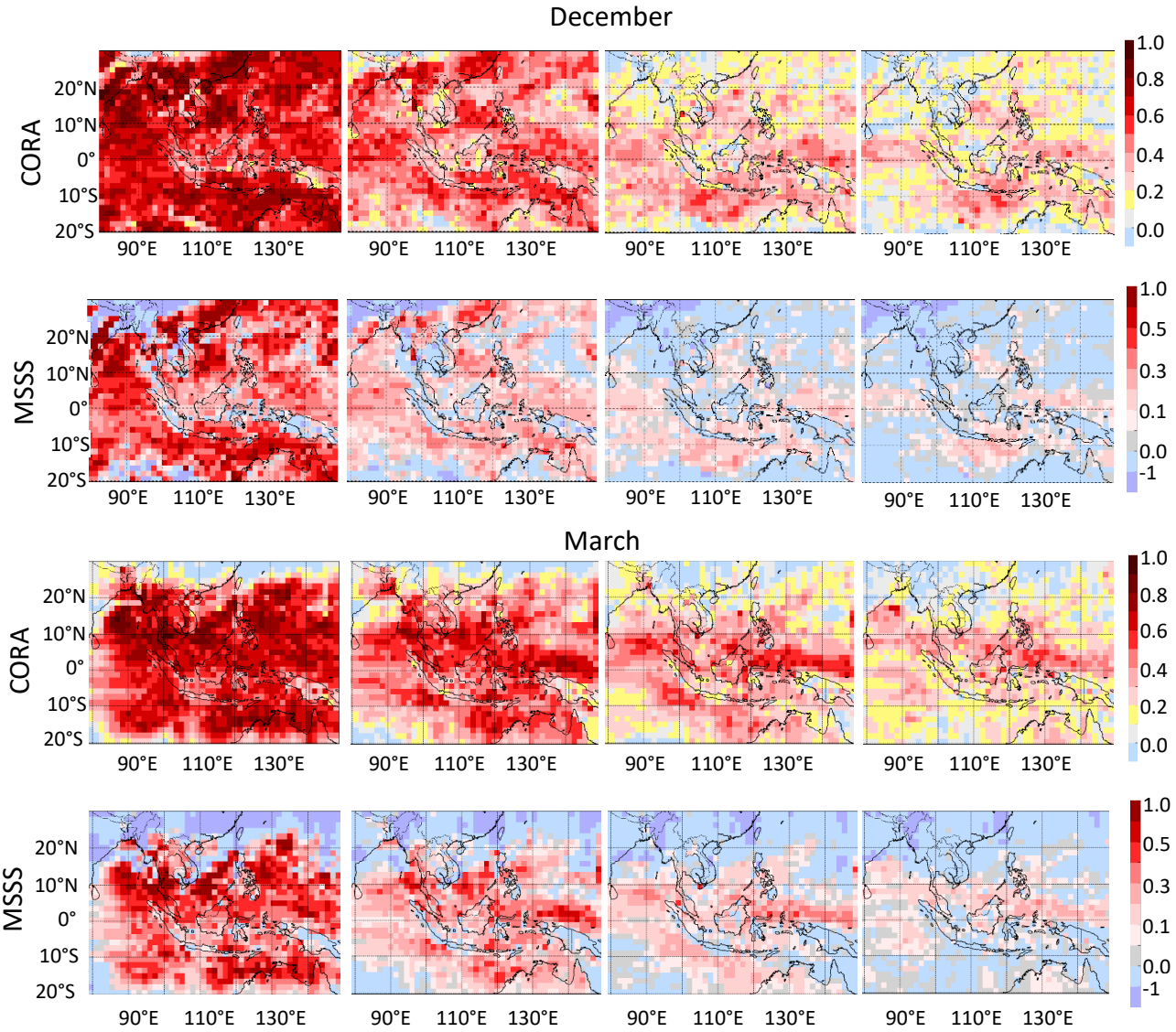

Figure 4 CORA and MSSS for December (top two rows) and March (bottom two rows) at lead times 1-4.

absolute difference, between the anomalies. The MSSS skill score for lead times 3 and 4 is generally low (<0.2) for the region studied, although there is still a slight positive correlation for CORA.

The skill over the ocean appears to be higher than over land for longer lead times in December (Figure 4). The Indian Ocean west of northern Sumatra and south of Java, along with the Java Sea and equatorial western Pacific Ocean, have the highest skill, while there is little to no skill over the Malay Peninsula, Sumatra, and Borneo. For March, the band of highest skill shifts further north, similar to the migration of the Intertropical Convergence Zone. This northward shift in skill also corresponds to an increase in the skill over the Malay Peninsula, possibly explaining why the March case study performed better than the January case study in 2004.

General Discussion

The analysis of the S2S forecasts skill depends on the quality of observation data. Comparing the satellite data used for forecast verification with the observations by the rain gauges, the weekly totals in Table 2 show discrepancies between the datasets. While differences would be expected between area-averaged (gridded) products and those from point-based rain gauges, TRMM aligns better with the rain gauges, apart from March 2004 where TRMM records 210 mm less rainfall (weekly total) than the rain gauge average. CHIRPS had similar values for the January 2004, December 2006, and January 2011 case studies, even though the rain gauge values varied by 330 mm between these events. CHIRPS also underestimated the March 2004 event rainfall by 300 mm. Although, the rainfall anomalies in Figure 3 show above-average

rainfall for both satellite-derived datasets. Therefore, while skill scores would likely differ based on observational dataset, the pattern is expected to be similar.

The skill scores and the case studies highlight the difficulty in using the deterministic values directly for lead times 3 and 4. One reason for the difficulty could be calculating the anomaly using the ensemble mean, rather than individual ensemble members. Over longer lead times, the spread between ensemble members grows, reducing the ensemble mean anomaly. An improvement for extreme rainfall could be to assess the number of ensemble members that indicate extreme rainfall, rather than the average. At lead times 3 and 4, the probability of extreme rainfall may be of more use than the ensemble mean.

The presence of large-scale drivers may explain the good predictability for the ECMWF model for the chosen case studies. In each case, there was either a La Niña or the wet phase of the MJO. Li and Robertson (2015) found that the presence of MJO and ENSO may provide 'windows of opportunity' for high predictability. Identifying the key situations when there is better predictability, along with individual ensemble members, may be more useful than using the deterministic ensemble mean forecasts directly.

Finally, while the results indicate that above-average rainfall was forecasted for the four extreme hydro-meteorological events, further study is needed to determine the frequency of occurrence of such forecasts. Determining the number of false positives (heavy rain forecasted when none occurred) along with the false negatives (heavy rain occurred but was not forecasted), would help to more comprehensively determine the usability of the S2S forecasts.

CONCLUSION

Four extreme hydro-meteorological events were selected to assess subseasonal forecasts for southern Malay Peninsula. The case studies occurred during or after the Northeast Monsoon and were associated with cold surges. Each event was associated with a La Niña event or wet phase of the MJO. Forecasts for each case study were assessed at four lead times (one to four weeks) using ECMWF re-forecasts from the S2S Project database. CORA and MSS values were used to determine the overall skill for each month and lead time.

Overall, the ECMWF ensemble mean predicted well each of the case studies at lead times of up to two weeks. The skill for lead times 1 and 2 was also high based on the CORA and MSSS skill scores for December and March from the re-forecasts. Therefore, these events suggest that S2S forecasts have the potential for use in early warning of extreme hydro-meteorological events up to two weeks for the region, which may provide valuable information for planning and activation of resources in disaster mitigation.

The ability of the forecast to predict the case studies at lead times 3 and 4 depended on the event. The presence of either La Niña or MJO for each of the events possibly increased the predictability for the case studies. However, in the case of the January 2004 event, the rainfall anomaly pattern was not well predicted past lead time 2, possibly due to the difficultly in predicting cold surges. The skill based on CORA and MSSS was also low at lead times 3 and 4. Therefore, while there is some skill at lead times 3 and 4, the forecasts should not be used directly, but can potentially be used as a guide for preliminary warning through risk-based, probabilistic forecasts instead.

Thus, future work should consider not only the ensemble mean, as assessed here, but also the individual forecasts and probabilistic forecast products. This is particularly important for lead times 3 and 4, where the deviation between the ensemble member forecasts is larger and hence the ensemble mean average anomalies are reduced. The individual forecasts collectively may better capture the probability of extreme rainfall at longer lead times, particularly of interest when considering early warning for flooding in the southern Malay Peninsula.

REFERENCES

BoM (2018) Madden-Julian Oscillation (MJO). Available at: www.bom.gov.au/climate/mjo, last accessed 4 September 2018.

Blumenthal, M.B., Bell, M., del Corral, J., Cousin, R., Khomyakov, I. (2014) IRI Data Library: enhancing accessibility of climate knowledge. *Earth Perspectives*, 1:19.

DREF (2007) Malaysia: Floods. Final Report for DREF Bulletin no. MDRMY001. Available at: reliefweb.int/sites/reliefweb.int/files/resources/7D3B1EF2384E9D2749257325001FA32E-Full_Report.pdf, last accessed 16 July 2018.

Dartmouth (2018a) 2004 Flood Archive. Dartmouth Flood Observatory. Available at: www.dartmouth.edu/

~floods/Archives/2004sum.htm, last accessed 12 September 2018.

Dartmouth (2018b) 2006 Flood Archive. Dartmouth Flood Observatory. Available at: www.dartmouth.edu/~floods/Archives/2006sum.htm, last accessed 12 September 2018.

Funk, C., Verdin, A., Michaelsen, J., Peterson, P., Pedreros, D., Husak, G. (2015) A global satellite-assisted precipitation climatology. *Earth System Science Data*, 7:275–287.

Huffman, G. J., Adler, R. F., Bolvin, D. T., Gu, G. J., Nelkin, E. J., Bowman, K. P., Hong, Y., Stocker, E. F., Wolff, D. B. (2007) The TRMM multisatellite precipitation analysis (TMPA): Quasi-global, multiyear, combined-sensor precipitation estimates at fine scales. *Journal of Hydrometeorology*, 8:38–55.

Kalnay, E., Kanamitsu, M., Kistler, R., Collins, W., Deaven, D., Gandin, L., Iredell, M., Saha, S., White, G., Woollen, J., Zhu, Y. et al. (1996) The NCEP/NCAR 40-Year Reanalysis Project. *Bulletin of the American Meteorological Society*, 77:437–472.

Li, S., Robertson, A.W. (2015) Evaluation of Submonthly Precipitation Forecast Skill from Global Ensemble Prediction Systems. *Monthly Weather Review*, 143:2871–2889.

Lim, S. Y., Marzin, C., Xavier, P., Chang, C., Timbal, B. (2017) Impacts of Boreal Winter Monsoon Cold Surges and the Interaction with MJO on Southeast Asia Rainfall. *Journal of Climate*, 30:4267–4281.

Reliefweb (2018) Malaysia: Floods - Jan 2011. Available at: reliefweb.int/disaster/fl-2011-000021-mys, last accessed 19 July 2018.

Tan, M. L., Chua, V.P., Li, C., Brindha, K. (2018) Spatiotemporal analysis of hydro-meteorological drought in the Johor River Basin, Malaysia. *Theoretical and Applied Climatology*, doi: 10.1007/s00704-018-2409-5.

Tan, M. L., Ibrahim, A. L., Yusop, Z., Duan, Z., Ling, L. (2015) Impacts of land-use and climate variability on hydrological components in the Johor River basin, Malaysia. *Hydrological Sciences Journal,* 60:873–889.

Turkington, T., Timbal, B., Rahmat, R. (2018) The impact of global warming on sea surface temperature based El Nino-Southern Oscillation monitoring indices. *International Journal of Climatology*, doi: 10.1002/joc.5864.

Vitart, F., Ardilouze, C., Bonet, A., Brookshaw, A., Chen, M., Codorean, C., Déqué, M., Ferranti, L., Fucile, E., Fuentes, M. et al. (2017) The Subseasonal to Seasonal (S2S) Prediction Project Database. *Bulletin of the American Meteorological Society*, 98:163–173.

Xavier, P., Rahmat, R., Cheong, W.K., Wallace, E. (2014) Influence of Madden-Julian Oscillation on Southeast Asia rainfall extremes: Observations and predictability. *Geophysical Research Letters*, 41:4406–4412.

WAS THE SINGAPORE JANUARY 2018 COLD SPELL RECORD-BREAKING?

Junhua Yang[1], Pei Yun Teo[2], Bertrand Timbal[1]

[1]Climate Modelling and Prediction Section, Centre for Climate Research Singapore, [2]Department of Geography, National University of Singapore

INTRODUCTION

In mid-January 2018, Singapore experienced a prolonged period of low temperatures due to persistent rainfall associated with a cold surge during the Northeast Monsoon season. This period of low temperatures across the island, which lasted for about 5 consecutive days from the 10th to 14th January, was unusually long. Changi Climate Station reported that the daily maximum temperature ranged from 23.7°C to 26.7°C, while the daily minimum temperature ranged from 21.3°C to 22.8°C during this event. Both daily maximum and minimum temperature ranges were well below the past 30-year mean values for January, which are 30.6°C and 24.2°C respectively.

The low temperatures together with the long duration attracted considerable media interest and became a talking point for that week, as an event of this magnitude had not been recorded in recent decades. The media reported people having to rely on wearing winter clothes (The Straits Times 2018a), an oddity in Singapore, a country well-known for its warm and humid climate throughout the year. Some small-scale annoyances on people's daily life were also reported: e.g. pre-school children having to spend more time indoors or air coolers usually cooling in alfresco dining for customers set to blow warm air instead (The Straits Times 2018b).

Cold spells, also known as cold waves or cold snaps in some regions, are known to affect many parts of the extra-tropical world (e.g. North America, Europe and East Asia) where they cause large, sharp drops in temperature with life-threatening consequences. While relatively more benign in Singapore, these cold spells, as the January 2018 event demonstrated, do impact business operations and the daily activities of Singaporeans. Like other cold spells around the world in recent times, they raise questions and misconceptions among the general population on the validity of the global warming trend due to increased greenhouse gas emissions.

The long-term trend notwithstanding, cold spells could be caused by naturally occurring climate modes of variability, such as El Niño–Southern Oscillation (ENSO). ENSO events can have impact on the frequency of cold surges during the Northeast Monsoon (Wu and Leung 2009) and it is plausible that the occurrence of persistent rainfall during cold surges could in turn lead to cold spells over Singapore. This possible ENSO-Cold Spell connection is worthy of being investigated as well as the long-term trends.

From a meteorological perspective, it is of interest to local weather forecasters to gain a better understanding of cold spell events and their relationship with large-scale cold surges during the Northeast Monsoon (from late November to March). While rainfall patterns associated with cold surges have already been studied by many researchers (e.g. Lim et al. 2017), to the best of the authors' knowledge, there are no previous systematic studies on temperature patterns in Singapore associated with cold surges. This study aims to fill the current gap.

In this study, the historical temperature records from existing MSS observation stations are examined to identify and characterise past cold spell events in Singapore. In the process, two definitions of cold spells appropriate in the Singapore context were tested. Based on these definitions, a climatology of cold spell events is established including the length, frequency, and spatial variability of the events across Singapore. In relation to the climatology, the significance of the January 2018 cold spell is discussed further.

DATA AND METHOD

Data used to identify cold spell events in this study are from five manned weather stations, located in Changi, Paya Lebar, Seletar, Sembawang and Tengah, for which sufficiently long records exist (their exact location is documented in Figure 5). Daily maximum and minimum temperatures were recorded at each station, all currently in operation but started in different years. Paya Lebar has the longest records (since August 1955), while Sembawang is the most recent station (since April 1986). Besides these five stations, historical data from Kallang (June 1934 to August 1955) were included to

analyse longer-term variability and trends despite the station being the sole measurement prior to 1955 and with a data gap from 1942 to 1947 owing to the Japanese Occupation during World War II.

Two different criteria were tested to identify cold spell events: one based on daily maximum temperature (Tmax) only and the other based on the average between daily minimum (Tmin) and maximum temperature (Tavg = [Tmax+Tmin]/2). The motivation to use both criteria is that it is unclear, between minimum and maximum temperature variables, which will impact the general population more.

In addition, the severity of the events was tested using two thresholds to differentiate 'cool spell' and 'cold spell' events, the former being less severe. A cool spell event is recorded when either the daily Tmax is below 27°C or daily Tavg is below 25°C and the event persists for at least 2 consecutive days. Similarly, a cold spell event is recorded when either the daily Tmax is below 26°C or the daily Tavg is below 24°C. The cool spell thresholds represent the lowest 2.5% of the temperature records at all stations and the cold spell thresholds represent the lowest 1%. In Europe, the Copernicus European Drought Observatory (EDO) uses the 10th percentile daily threshold for both Tmax and Tmin for their definition of extreme low temperature cold waves (EDO 2018). The Japan Meteorological Agency on the other hand monitors the weekly mean temperature anomaly and checks if it exceeds 3 times the 30-day standard deviation (WMO 2018). There are no unique criteria or thresholds for cold spell/cold wave, and different countries located in different geographical regions tend to have their own criteria and thresholds to suit their own local requirements. In this study, we have chosen a far more stringent threshold to recognise the fact that, due to the tropical climate of Singapore, only the most severe of events are expected to impact the daily activities of the general public. This was a subjective choice based on the public perception that emerged during the January 2018 cold spell event and a starting point to be analysed in this paper.

Two data issues needed to be addressed before applying these criteria: 1) biases due to shifts in the locations of temperature sensors and 2) missing data.

According to the available metadata, three weather stations (Paya Lebar, Seletar, and Tengah), shifted the location of their temperature sensors. Paya Lebar's temperature sensor was shifted to a rooftop on the 19th August 1981, Seletar's sensor was also moved to the rooftop on the 14th November 2011, while Tengah's sensor was elevated to a higher ground from 7.6 m to 16.8 m in June 1986. In order to evaluate if there were significant impacts due to these shifts, the daily minimum (or maximum) temperature records were first averaged into yearly data and grouped into pairs of 5-year intervals for comparison prior to and after the documented change in the instrumentation's location.

For example, the Seletar station was relocated in 2011, therefore the differences compared are between the mean for 5-year intervals before (2006–2010) and after (2012–2016) the shift. This difference is then compared against the median of the distribution of all the differences computed from all adjacent pairs of 5-year intervals in Seletar's entire record, excluding intervals containing the year of the shift, thus providing an estimate of the distribution of plausible shifts between 5-year periods in the full record. The result for the impact of the location shift on Seletar's daily minimum temperature is shown in Figure 1.

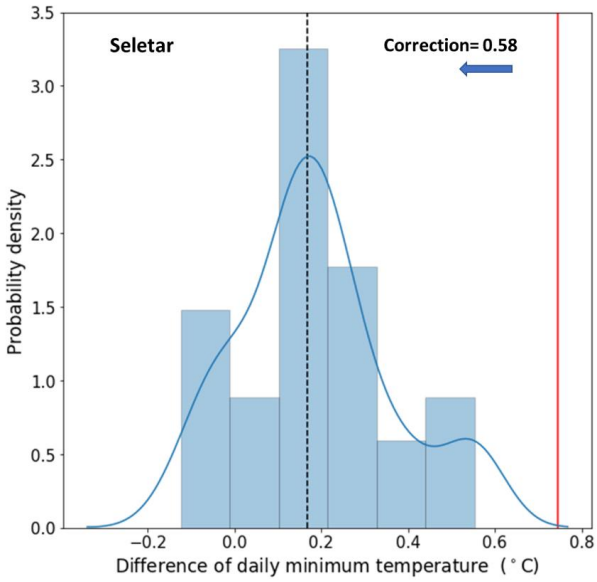

Figure 1 Distribution of the difference in the mean daily Tmin at Seletar station of adjacent non-overlapping 5-year intervals. The dashed vertical line represents the median (0.17) of the distribution. The red vertical line (0.74) represent the increase in temperature after the shift. The difference between the two values (0.58) is used to correct the observations post 2011 to account for the effect of the shift in instrumentation over time.

In the case of Seletar's daily minimum record (Figure 1), the shift due to the change of location resulted in a large increase in the temperature (indicated by the position of the vertical red line) far larger than the median (dashed black line) estimated from all possible 5-year periods and larger than all other 5-year differences; thus indicating that the shift is significant compared to random differences between 5-

year periods. The shift in the time series was corrected by removing from all daily minimum temperature recorded after 2011 0.58°C, the difference between the shift when the instrument was moved and the median of all other 5-year shifts.

The same procedure was applied to Paya Lebar and Tengah's dataset for both minimum and maximum time series. With this method, it was found that shift of sensor locations had significant impact on Seletar's minimum and maximum temperature and Tengah's minimum temperature. Temperature time series were corrected accordingly and in the case of Seletar, data after the shift was corrected as the roof top location is less suitable than the earlier ground location, but in the case of Tengah, where both locations are suitable being at ground level, the correction was applied to the earlier part of the record in order to align with on-going measurements (Table 1).

Another issue with the datasets is that there were no observations at Sembawang manned station during the weekend starting from September 2017 onwards. This issue was remedied by comparing observations from other stations. If at least 3 stations recorded a cool/cold spell event, it was assumed that Sembawang would have also recorded the event.

In addition to Singapore's temperature observations, this study makes use of a classification of ENSO events and years using the detrended (removal of the background tropical warming signal) Nino3.4 Sea Surface Temperature index (Turkington et al. 2018). ENSO year (from June to May) are classified in one of the three states: El Niño, La Niña or Neutral. This classification was used to find out if cool spells in Singapore tend to favour certain ENSO states.

The region's climate is influenced by drivers at various spatial scales. Large-scale atmospheric drivers include ENSO and the Indian Ocean Dipole. The Madden-Julian Oscillation (MJO), one of the main subseasonal drivers globally, tends to bring more rainfall during Phases 2–4 and drier conditions during Phases 6–8 for the region (Xavier et al. 2014). During the Northeast Monsoon, strong winds over the South China Sea associated with southward intrusions of the Siberian high bring increased convection over the Maritime Continent, termed cold surges (Lim et al. 2017). When cold surges and the MJO occur at the same time, the rainfall pattern tends to more closely resemble a cold surge, with the MJO increasing the extreme rainfall response in the region in Phases 2–4 (Lim et al. 2017).

RESULTS AND DISCUSSION

The number of cool and cold spell events observed at the five stations since 1971 are summarised based on the Tmax and Tavg criteria (Figure 2). Up to five cool spells have been observed in one year (1973 in Paya Lebar based on the Tavg criteria) but usually there are no more than two cold spells (in several locations and years). Overall, the distribution of cool and cold spells is broadly similar between the two different criteria (Tmax and Tavg) indicating that both criteria are acceptable and can be chosen depending on what impact is to be considered. Some differences exist but for brevity, we focus the discussion on the climatology based on the Tmax criterion.

Singapore experienced a larger number of cool and cold spell events back in the 1980s to the mid-1990s (Figure 2); prior to this in the 1970s, less events are apparent although it is difficult to be definitive as less stations were in operation. After the mid-1990s, widespread (observed at all five stations) cool and cold spell events became relatively infrequent. Such widespread events occurred only three times: in 1995, 2011, and 2018. Cool spells in Singapore are predominantly nationwide phenomena and localised cool spells are much less common. From January 1987 to April 2018, when all five stations are in operation, almost three-quarters (73%) of all cool spell events were simultaneously observed by at least three out of the five stations.

Table 1 Summary of the corrections applied to remove changes in temperature measurements at Seletar and Tengah station due to sensor location shifts.

Station	Bias Measurement	Location Shift's Year	Note	Correction (°C)	Applied Correction
Seletar	Daily Tmax	2011	Change to rooftop after 2011	0.69	Records after 2011 were corrected downwards
Seletar	Daily Tmin	2011		0.58	
Tengah	Daily Tmin	1983	Elevation raised from 7.6m to 16.8m on higher ground	-0.40	Records before 1986 were corrected downwards

The length of a cool spell event can range from 2 to 6 consecutive days and a cold spell event can last from 2 to 4 consecutive days depending the criteria used (Figure 3 for Paya Lebar, the longest record available). Paya Lebar is representative of other locations as well since cool and cold spells affect many stations simultaneously. The bulk of the cool and cold spell events occurred during the Northeast Monsoon months and longer lasting events (4 to 6 consecutive days) are only observed in December and January, thus confirming the role of cold surges during the Northeast Monsoon in bringing anomalous cooler and wetter weather. Rare instances of cool spells did occur during the Southwest monsoon (July to September), although they were shorter (never exceeding 3 days) and never reached cold spell thresholds. Anecdotal evidence of the strong association of cold/cool spell with rainy weather in Singapore can be seen from the case of Paya Lebar station where for the past 20 cold spell events from 1955–2018, long duration rainfall was observed

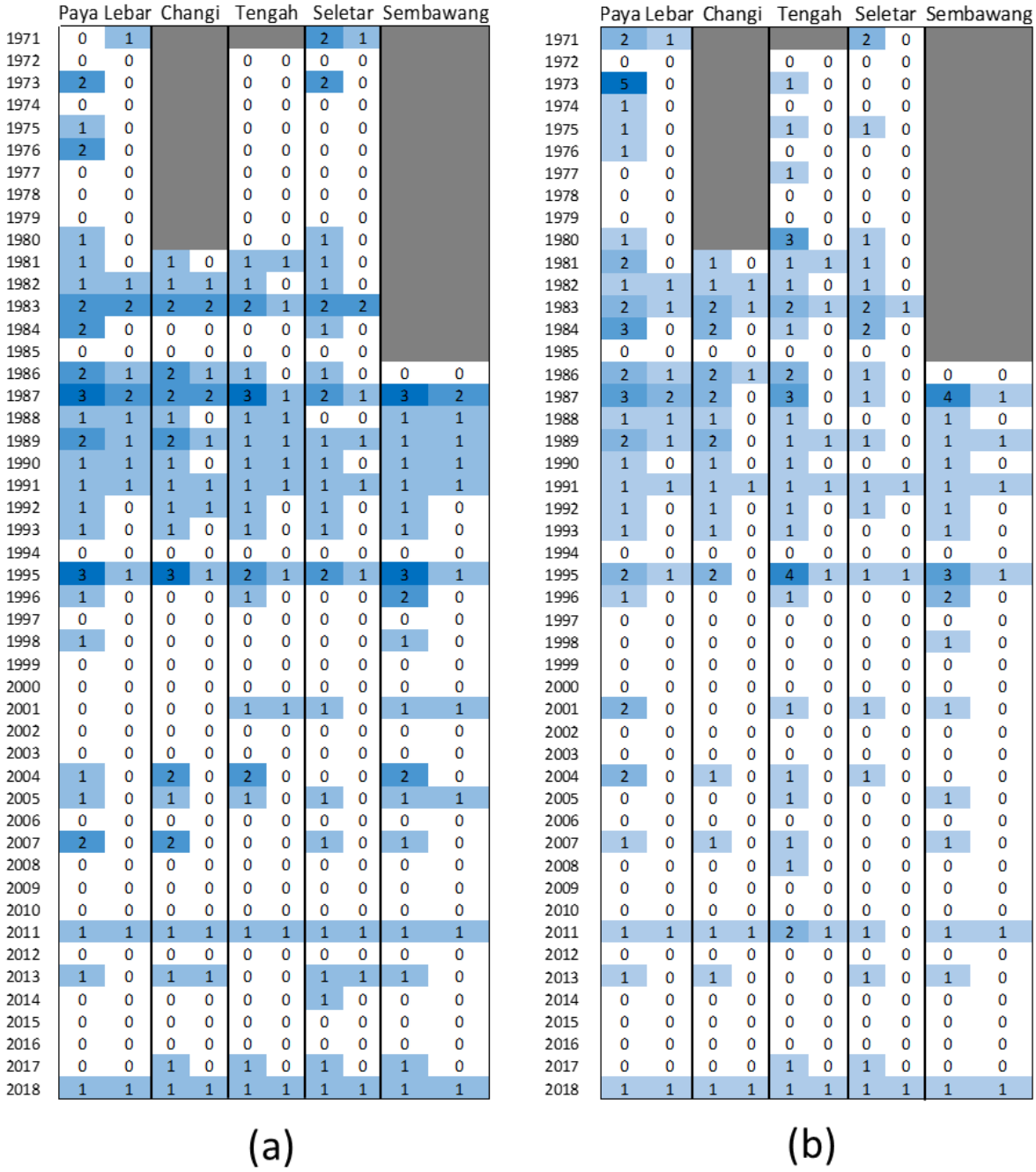

Figure 2 Distribution of the number of cool (left column) and cold (right column) spell events from 1971 to 2018 (up to April) for the five manned stations in Singapore, based on daily Tmax criteria (a) and on daily Tavg = [Tmax + Tmin]/2 criteria (b). Greyed out cells indicate that the particular station was not in operation.

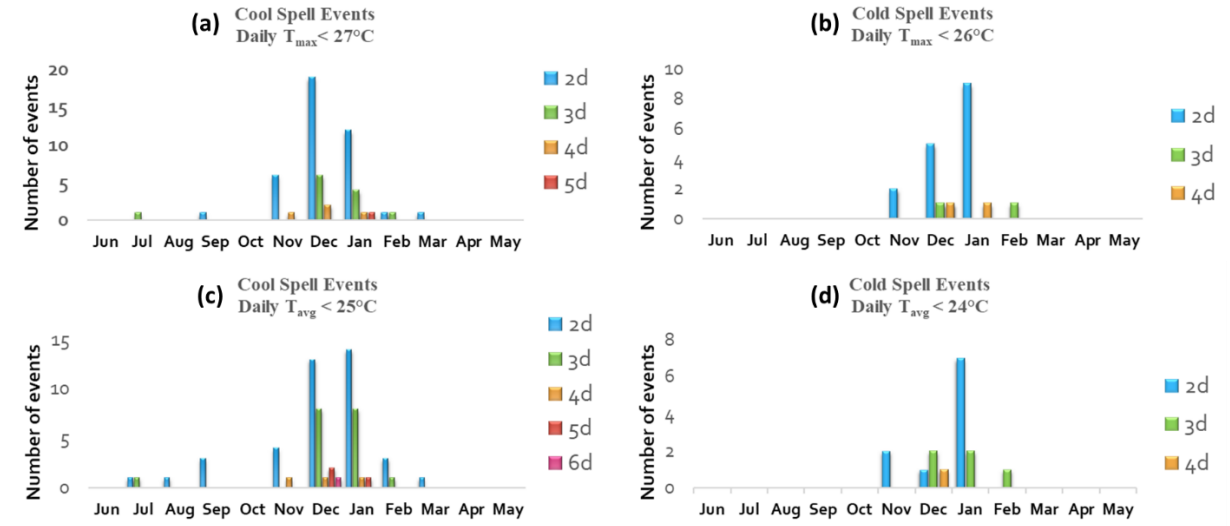

Figure 3 Annual distribution of cool (left) and cold (right) spell events and their durations (number of consecutive days) at Paya Lebar station (1955 to 2018) using different criteria: Tmax (top row: a and b) and Tavg = [Tmax + Tmin]/2 (bottom row: c and d). Events with longer durations are excluded from the shorter duration events thus avoiding double-counting.

during every single cold spell event. The observed total rainfall duration lasted from 19 hr to 57 ht throughout each cold spell event (2 to 4 days long).

Long-term trends and inter-annual variability are evaluated on an extended record from 1934 to present by combining Kallang's historical observations from 1934 to 1955 with Paya Lebar record from 1955 to current (Figure 4). Since 1995, cool spells have become rare in Singapore, although from 1934 to the early 1990s, there was no apparent trend. It is worth noting that in the meantime, Singapore went through a rapid warming trend from the 1970s to the mid-1990s of about 1.5°C, which is likely due to a combination of the on-going global warming trend and urbanisation (MSS 2016). From Paya Lebar's record, the number of cool days decreased from 9.0 to 5.4 days per year between 1959-1988 and 1989-2018. In the meantime, alongside the reduction in the number of days, a smaller proportion are observed as part of spells: from 31% to 26%. A similar reduction in total number of days and proportion of day forming parts of spells are observed for the cold threshold: from 3.6 to 2.3 days per year and from 27% to 19% of days being part of spells. As these days with the lowest temperatures are becoming rarer, they are less likely to extend spells of any duration. No significant relationship was found between the main mode of natural variability affecting the Western Maritime Continent and Singapore (ENSO) and the occurrences of cool/cold spells (Figure 4); a simple binning of cool spell days within each ENSO category revealed no meaningful or consistent differences between El Niño, Neutral, or La Niña years. Although, it is worth noting that no cool spells occurred during El Niño years after 1995. This may be related to the lack of long enough cold surges that occurred during those El Niño years (Lim et al. 2017). A deeper understanding of these factors however requires a separate study and is not addressed in this current work.

With this long-term climatological perspective, the January 2018 cold spell appears as an extremely

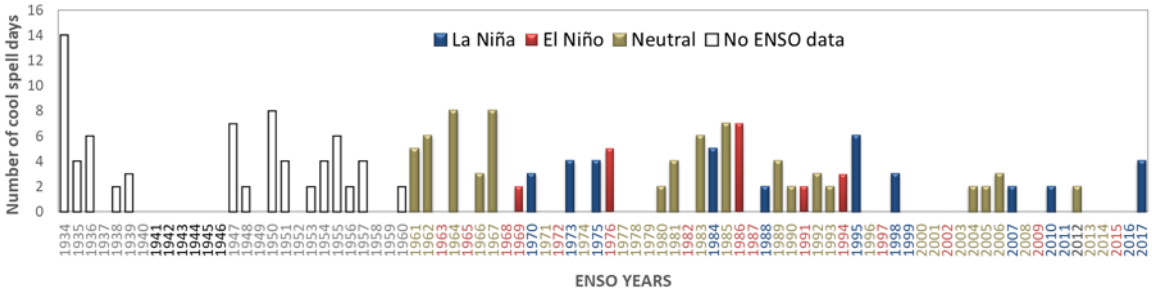

Figure 4 Annual count (the definition of the year is based on the ENSO cycle and are from June to May) of cool spell days (based on the Tmax criteria and at least two consecutive days for the days to be counted) from 1934 to 2017; data are from Kallang station from 1934 to 1954 (with a gap from 1941 to 1946) and from Paya Lebar after 1955. ENSO years (El Niño, Neutral and La Niña) are indicated by colour code and available from 1961 onward (from Turkington et al. 2018).

severe case when considering the various aspects (total duration, temperature, and spatial extent) together. Singapore had not experienced a similar case in the past two decades. As a cold spell (daily Tmax < 26°C), the 2018 event lasted for 4 days, or as a cool spell (daily Tmax < 27°C) the event lasted for 5 days, making the event unusually long and widespread in the historical context (Figure 5). When the cool threshold is used, the event was record-breaking in duration for Sembawang (5 days) and equal the previous record for Tengah, Changi, and Seletar (at either 4 or 5 days). In the context of the on-going warming trend, it was even more remarkable when the cold threshold is used: either record-breaking or equal the longest at 4 stations (Changi, Seletar, Tengah, and Sembawang). In summary, the combination of the magnitude of the temperature anomalies, the duration of the spell, and widespread nature of the January 2018 event made the event quite remarkable. Even more so after nearly two decades of no similar events.

CONCLUSION

Cool/cold spells, based on the definitions chosen in this study, are quite rare in Singapore. In any given year, there are usually no more than 1 or 2 events and up to 3 or 5 events for a few exceptional years all before 1995. In most years, there are no such events. Cold spells are predominantly widespread and can be regarded as nationwide phenomena. Cool spells can last from 2 to 6 consecutive days, while cold spells can last from 2 to 4 days. Both occur mostly during the Northeast Monsoon (late November to March) and are likely associated with prolonged rainfall during cold surges. Some cool spells do occur during the Southwest Monsoon but are extremely rare and do not last for more than 3 days; no cold spells have ever occurred during the Southwest Monsoon. Of note, there seems to be no particular prevalence for cold spell events in relation to ENSO variability.

In the historical context, the January 2018 cold spell is indeed remarkable in consideration of its duration, temperature, and widespread nature; no similar events had been seen since the early 1990s. During the 1980s to the mid-1990s, there were generally more cool and cold spell events than during any other period, but they became relatively infrequent following a period of rapid warming recorded across the MSS network of manned temperature stations from the 1970s to the mid-1990s. Therefore, it is not surprising that the 2018 event made so many local newspaper headlines and that many Singaporeans reacted to it.

This simple climatological analysis provided a basis for understanding these meteorological events

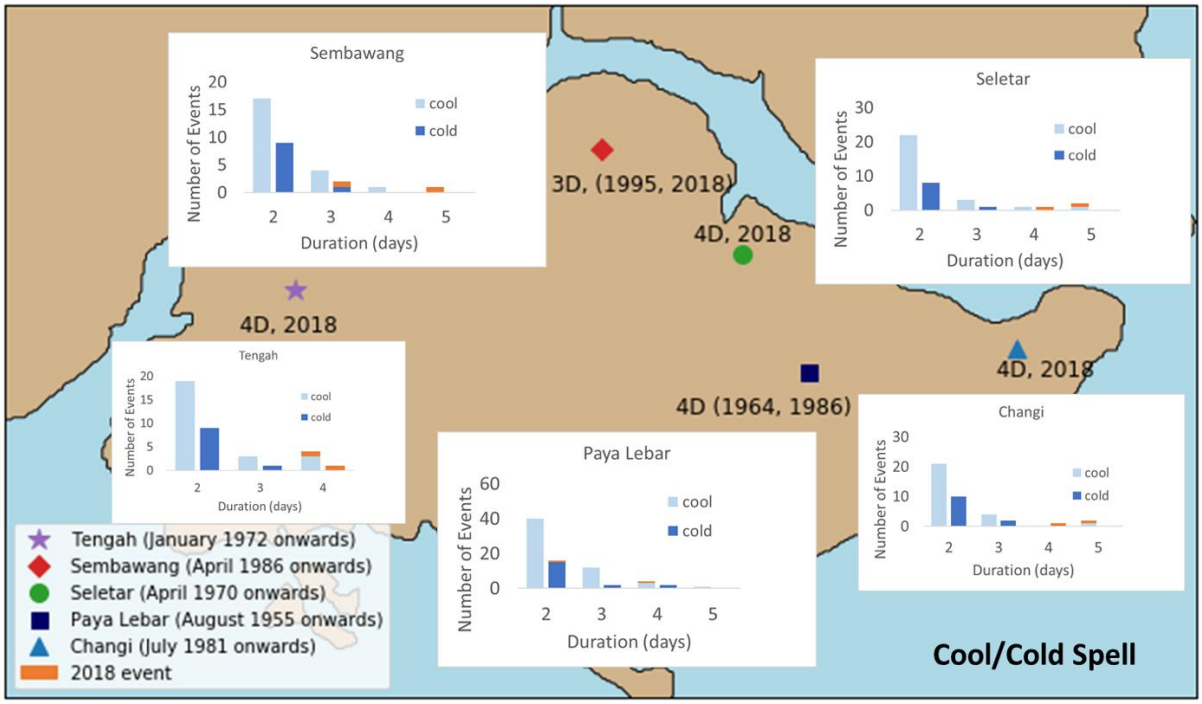

Figure 5 The January 2018 cold spell event as observed at the five stations in Singapore. The number of cool/cold spell events observed at for various durations is shown for comparison. The duration of the longest cold spell event together with the year of occurrence is also indicated at each station. The duration of the January 2018 cold spell event broke the records at three stations (Changi, Seletar, and Tengah).

and future work of interest could improve our understanding of that climatology in relation to large-scale meteorological events (the propagation of MJO events, Northeast Monsoon cold surges, wet spells etc.). It would also be valuable to study the potential impact of future projected warming in Singapore on the observation of future cold spells. Analysis of the Singapore 2nd National Climate Change Study (Gordon et al. 2015) indicated that the Northeast monsoon cold surges may increase in intensity (Marzin and Lim personal communication); therefore, it opens up the possibility that despite global warming combined with localised urbanisation related warming, Singapore may continue to experience rare cold spells in the future.

REFERENCES

EDO (2018) Heat and Cold Wave Index (HCWI). Available at: edo.jrc.ec.europa.eu/documents/factsheets/factsheet_heatColdWaveIndex.pdf, last accessed 16 November 2018.

Gordon C., Cheong, W.K. Marzin, C., Rahmat, R. (2015) Singapore's Second National Climate Change Study - Climate Projections to 2100 - Report to Stakeholders. Centre for Climate Research Singapore. Available at: ccrs.weather.gov.sg/wp-content/uploads/2015/04/Publications-Second-National-Climate-Change-Study-Report-for-Stakeholders.pdf, last accessed 11 December, 2018.

Lim, S. Y., Marzin, C., Xavier, P., Chang, C., Timbal, B. (2017) Impacts of Boreal Winter Monsoon Cold Surges and the Interaction with MJO on Southeast Asia Rainfall. *Journal of Climate*, 30:4267–4281.

MSS (2016) Annual Climate Assessment Report. Available at: www.weather.gov.sg/climate-annual-climate-reports, last accessed 28 September 2018.

The Straits Times (2018a) Last Week's Cool Spell was Singapore's longest in a decade. January 19, 2018. Available at: www.straitstimes.com/singapore/environment/last-weeks-cool-spell-was-singapores-longest-in-a-decade, last accessed 27 September 2018.

The Straits Times (2018b) The Big Chill: Coping with the cold and rain in Singapore. January 11, 2018. Available at: www.straitstimes.com/singapore/environment/the-big-chill-coping-with-the-cold-and-the-rain-in-singapore, last accessed 27 September 2018.

Turkington, T., Timbal, B., Rahmat, R. (2018) The impact of global warming on sea surface temperature based El Nino-Southern Oscillation monitoring indices. International Journal of Climatology, doi: 10.1002/joc.5864.

WMO (2018) Guidelines on the definition and monitoring of extreme weather and climate events. Available at: www.wmo.int/pages/prog/wcp/ccl/documents/GUIDELINESONTHEDEFINTIONANDMONITORINGOFEXTREMEWEATHERANDCLIMATEEVENTS_09032018.pdf, last accessed 16 November 2018.

Wu, M.C., Leung, W.H. (2009) Effect of ENSO on the Hong Kong winter season. *Atmospheric Science Letters*, 10:94-101.

Xavier, P., Rahmat, R., Cheong, W.K., Wallace, E. (2014) Influence of Madden-Julian Oscillation on Southeast Asia rainfall extremes: Observations and predictability. *Geophysical Research Letters*, 41:4406–4412.

DEVELOPMENT OF A MACHINE-LEARNING NOWCASTING SYSTEM

AT THE METEOROLOGICAL SERVICE SINGAPORE

Xiangming Sun[1] Erik Becker[1] Sijin Zhang[2] Xiang-Yu Huang[1] Quang Van Doan[3]

[1]Research to Operations, Centre for Climate Research Singapore, [2]MetService, New Zealand, [3]Weather Modelling Development, Centre for Climate Research Singapore

INTRODUCTION

Precipitation is one of the most significant meteorological phenomena that impacts our daily lives and is notoriously difficult to predict, due to its high variability in space and time. Precipitation patterns range from isolated convective thunderstorms that last only a few minutes, to large synoptic-scale systems that last for days. While the characteristics of the latter makes it easier to resolve within Numerical Weather Prediction (NWP) models, the dynamical processes of thunderstorms prove to be a greater challenge. However, it is possible to forecast such localised thunderstorms with reasonable accuracies at very short lead times.

According to the World Meteorological Organization, the term nowcasting refers to the current weather situation and the forecast of those observed conditions, typically between a 0- and 2-hour lead times. Nowcasting has always been a challenge for the NWP community. One reason is the model's inability to accurately represent the state of the atmosphere due to the lack of, as well as errors in atmospheric observations. Another reason is that the tolerance for location and timing errors with forecasted precipitation is very low. Furthermore, nowcasting applied to precipitation usually has a high spatial resolution with a high expectation of the location and timing accuracy of the forecast, which is a great challenge to NWP models. Nowcasting clearly requires a different approach to be of value (Sun et al. 2014).

Since the 1960s, a number of nowcasting systems that rely on radar observations have been developed, with two main strategies used: qualitative cell/object-based tracking systems (Dixon and Wiener 1993) and quantitative grid-based tracking systems (Li and Lai 2004). A comprehensive review of operational nowcasting systems is covered in Reyniers (2008). Both cases are based on extrapolation of precipitation in time and space using available information. However, localised thunderstorms in tropical areas that are of short life cycle tend to grow and decay rapidly,which greatly limits the predictability from extrapolation-based nowcasting.

Thunderstorms frequently occur in Singapore all year round induced mainly by diurnal forcing from radiation and surface heat fluxes (Qian 2008). In Singapore, nearly every other day is a thunderstorm day (a day in which thunder is heard; Fong 2012). Many hazardous phenomena associated with thunderstorms such as flash floods, microbursts, lightning, and hailstorms make heavy rain warning a high priority in MSS. A nowcasting system is helpful to assist forecasters in issuing heavy rain warnings. The development of the nowcasting system kicked off in mid-2016 and by Mar 2017 the first working version was released. From Apr 2017 onwards efforts were put into fine tuning the system, making it robust to run in real-time. The following sections contain the methodology followed by system configuration and the results and discussion.

DATA AND METHOD

The Artificial Neural Network (ANN; McCulloch and Pitts 1943) was employed in modelling the nowcasting system considering its strength in addressing nonlinearity of a problem. Through the ANN, a model is trained by fitting time series of radar reflectivity to the one that immediately follows. Upon completion of the training, the model is ready to perform prediction by taking in the latest radar reflectivity to produce a series of future forecasts in an iterative manner: the newly produced reflectivity will be used to update the input to perform the prediction again and again until the desired forecast length is reached. The system was written in Python and the ANN modelling part is built based on the 'Scikit-learn' Python module (Pedregosa et al. 2011). The key parameters of the ANN modelling, such as number of hidden layers, training data time window, and forecast length, were determined via experimenting different values in order to find an optimised balance among fitness,

computation cost and feasibility for real-time usage. In the current configuration, 25 hidden layers, a training time window of 50 minutes, and the forecast length of one hour are being used. In the rest of the paper, the nowcasting system is referred to as the ANN-NCST, short for ANN-based NowCaSTing system.

The radar data used in the ANN-NCST are level two volume scan data of calibrated reflectivity from the operational dual-pol Doppler Weather Radar of MSS at Changi (Figure 1, star). The dual-pol echo type products are also used for quality control purpose. The radar data pre-processing includes re-gridding, removal of echoes from ground clutter and insects, and removal of isolated cells and other small values.

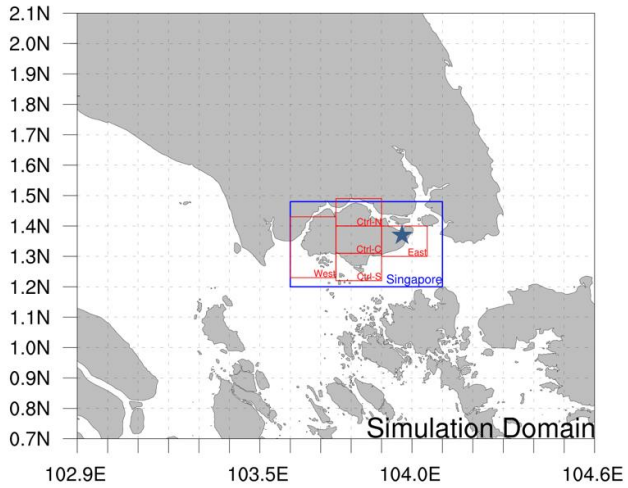

Figure 1 Various domains used, including the ANN-NCST simulation domain (the entire map), the five smaller regions over Singapore for verification only: Singapore (blue box), West (leftmost red box), Central-South (bottom middle red box), Central-Central (centre red box), Central-North (top middle red box) and East (rightmost red box); the star marks the location of the Changi radar.

The simulation domain of the ANN-NCST is illustrated in Figure 1 and the resolution is 2.0 km. At such a resolution, the Singapore domain (blue box in Fig. 1) with a dimension of 55×30 km^2 contains 348 (28×16) native resolution grid points. The ANN-NCST is scheduled to run twice per hour starting at 10 minutes after T0 (time = 0) due to the usual 6-minute delay of real-time radar observation. Given that the ANN-NCST needs another 5-9 minutes to complete the prediction and product uploading, the effective forecasts are from T+15 min and beyond for forecasters to reference in an operational setting.

A verification period of six months from 10 November 2017 to 9 May 2018 was chosen for two reasons. Firstly, the data quality and consistency are ideal in this period where the system configuration is frozen and the ANN-NCST was run twice per hour during this period. Secondly, the period covers two different seasons, the Northeast Monsoon (December to early March) and the first inter-monsoon season (late March till May), which provides opportunity to investigate system performances in two different types of seasons. In the Northeast Monsoon, rainfall caused by large-scale cold air invasions from South China Sea (cold surges) contributes as much rainfall over Singapore as localised thunderstorms. While rainfall associated with cold surges cannot be considered from just a large-scale perspective due to the interaction between mesoscale and local terrain features (Chang et al. 2016), the strong northeast wind helps the ANN-NCST to have more predictability in this season. Whereas during the inter-monsoon season, when environment wind is weak, localised and short-lived thunderstorms are dominant and are less predictable. The evaluation was carried out over two 3-month periods, months of (November to January (NDJ; large-scale rainfall dominant) and February to March (FMA; convective rainfall dominant), to increase the number of cases for verification.

Several verification domains illustrated in Figure 1 were used, including the entire simulation domain and much smaller ones over Singapore Island, which were defined from forecaster's perspective. Over the entire simulation domain, histograms and the Fractions Skill Score (FSS; Roberts and Lean 2008) were examined. A histogram provides intuitive overview on forecast bias across different thresholds whereas FSS is a good measure for spatial accuracy of precipitation forecasts (Mittermaier and Roberts 2010), as well as a better candidate to demonstrate benefits of kilometre-scale forecast of precipitation over traditional methods (Mittermaier 2014). Following Roberts and Lean's 2008 paper, a simplified calculation of FSS is given by Eq. (1), corresponding to the length scale of 2*n* km (as the resolution is 2 km and where *n* is the number of grid boxes at the particular length scale).

$$FSS = 1 - \frac{\frac{1}{N}\sum(f_m - f_o)^2}{\frac{1}{N}\sum {f_m}^2 + \frac{1}{N}\sum {f_o}^2} \quad (1)$$

where *N* is the total number of valid grid points in the domain; f_m is the forecasted rain cover fraction (Eq. 2) and f_o (Eq. 3) is observed rain cover fraction. Both fractions are defined with respect to the box spanned by *n*×*n* native grid points.

$$f_m = \frac{n_m}{n^2} \quad (2)$$

$$f_o = \frac{n_o}{n^2} \quad (3)$$

Several length scales were used in this study. They were selected such that the area of the square doubles each time length scale increases. The smallest length scale is 2 km, the native resolution, and the largest one is 270 km when FSS tends asymptotically to a value that is solely determined by bias (Eq. 7; Roberts and Lean 2008). The length scales in between are respectively 6 km, 10 km, 14 km, 22 km, 30 km, 46 km, 66 km, 94 km, 134 km, and 190 km.

Since FSS is calculated for categorical (yes/no) events, a threshold has to be determined. A set of reflectivity thresholds from low to high are selected based on hourly rain rates of our interest. The mapping from reflectivity to rain rate follows the study by Kumar et al. 2011 who proposed a relationship between radar reflectivity factor Z ($mm^{-6}m^{-3}$) and rain rate R (mm/h) by analysing drop size distribution data of convective rainfall over Singapore (Eq. 4).

$$Z = 328.64R^{1.29} \quad (4)$$

Ten thresholds have been considered: 0.1, 1.0, 2.0, 5.0, 10.0, 20.0, 30.0, 50.0, 70.0, and 100 mm/h. 50 mm/h was included because it is the heavy rain warning issuance criteria for MSS forecasters. Six other thresholds below 50 mm/h are chosen such that the exceeding probability decreases at about 10% intervals, based on a study of Singapore rainfall intensity distribution (Mandapaka and Qin 2013). A small value of 0.1 mm/h is set to differentiate yes/no rain events. 100 mm/h is chosen as the highest threshold as the exceeding probability is less than 0.01% and 70 mm/h is then determined as the logarithmic middle point between 50 mm/h and 100 mm/h. The same set of thresholds are used to bin the intensities to produce the histogram (Figure 2).

Table 1 Contingency table for calculating POD, SR, Bias, and CSI.

		Observed	
		Yes	No
Forecasted	Yes	a	b
	No	c	d

For smaller domains, FSS is not recommended as the domain dimension is closer to spatial error of forecasts (Skok and Roberts 2016). Metrics including Probability of Detection (*POD*; Eq. 5), Success Ratio (*SR*; Eq. 6), *Bias* (Eq. 7), Critical Success Index (*CSI*; Eq. 8) score and Critical Success Index Skill score (CSI_{skill}; Eq. 9) were investigated instead, all of which are derived from the contingency table (Table 1). All these metrics are commonly used to assess the operational usefulness of the forecasts.

$$POD = \frac{a}{a+c} \quad (5)$$

$$SR = \frac{a}{a+b} \quad (6)$$

$$Bias = \frac{a+b}{a+c} \quad (7)$$

$$CSI = \frac{a}{a+b+c} \quad (8)$$

$$CSI_{skill} = \frac{CSI - CSI_{ref}}{1 - CSI_{ref}} \quad (9)$$

where CSI_{ref} (Eq. 10) is derived using base frequency f_b, i.e. the fraction of observed rain cover.

$$CSI_{ref} = \frac{f_b}{1 - f_b} \quad (9)$$

Results and Discussion

Figure 2 shows the histograms of frequencies of different rain intensities from radar observations and forecasts of T+30 min and T+60 min over the entire simulation domain for the two seasons. The histograms

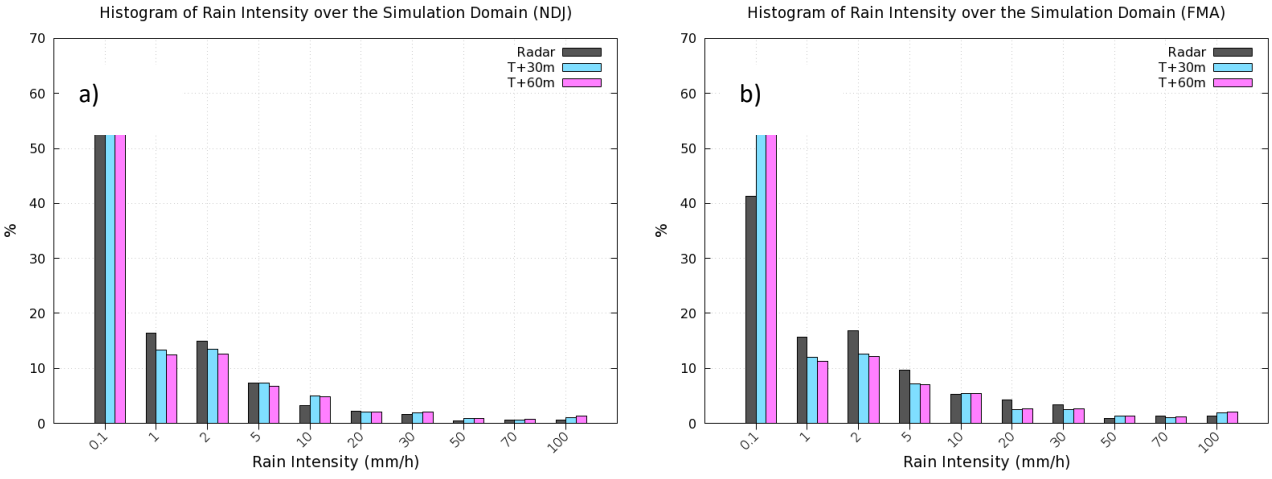

Figure 2 Histogram of frequencies of different rain intensities from radar observation (black) and forecasts of T+30 min (cyan) and T+60 min (purple) over different months for months of (a) NDJ and of (b) FMA.

indicate that the frequency distribution of intensities of T+30 min forecasts (cyan bars) is in good agreement with the observed (black bars) and so does that of T+60 min (purple bars) except slightly larger deviations from the observed than T+30 min forecasts. In general, the ANN-NCST does a good job in representing the intensity distribution across all thresholds up to the lead time of T+60 min. The wet-bias for the lightest rainfall (<1 mm/h) and the dry-bias in slightly heavier rainfall is found in both seasons, which indicates that the ANN-NCST cannot maintain the intensity structure over time, or more light rainfall forecasted that is supposed to be heavier. This over-forecasting of light rainfall is more evident in FMA season than in NDJ season, potentially due to the shorter life time of light rainfall in FMA season. While at the intense rainfall end, the ANN-NCST tends to maintain intense rainfall longer than observed, and we speculate this is most likely related to the partial fitting scheme of the training. More experiments are needed to look into this issue as it will lead to higher false alarm ratios.

Figure 3 plots FSS against different length scales, or different neighbourhood allowances for location error. Only plots of T+10 min and T+60 min are shown. From Figure 3, generally, FSS decreases over lead time and in most cases decreases as threshold increases. There are five exceptions out of the 120 cases that do not follow this rule. For example, in Figure 3a where FSS for threshold ≥ 70 mm/h and ≥ 100 mm/h are not always lower than lighter rain events. We believe this is because of the smaller sample size as all these five cases are of the highest two rain rates (70 mm/h and 100 mm/h).

When comparing the results for the two different seasons (left column vs right column, Figure 3), the NDJ season's forecast skill for heavier rainfall (threshold > 5 mm/h) drops much faster than in the FMA season over time. We speculate this performance difference is because there are more large-scale precipitation events in the NDJ season, featured by broader rain area, than in the FMA season where locally developed convections dominate with constrained rain areas. Thus, the higher intensity rainfall in NDJ accounts for a relatively smaller portion of total rain area. As a result, it is more difficult to capture the pattern of higher intensity rainfall in NDJ and hence the lower scores.

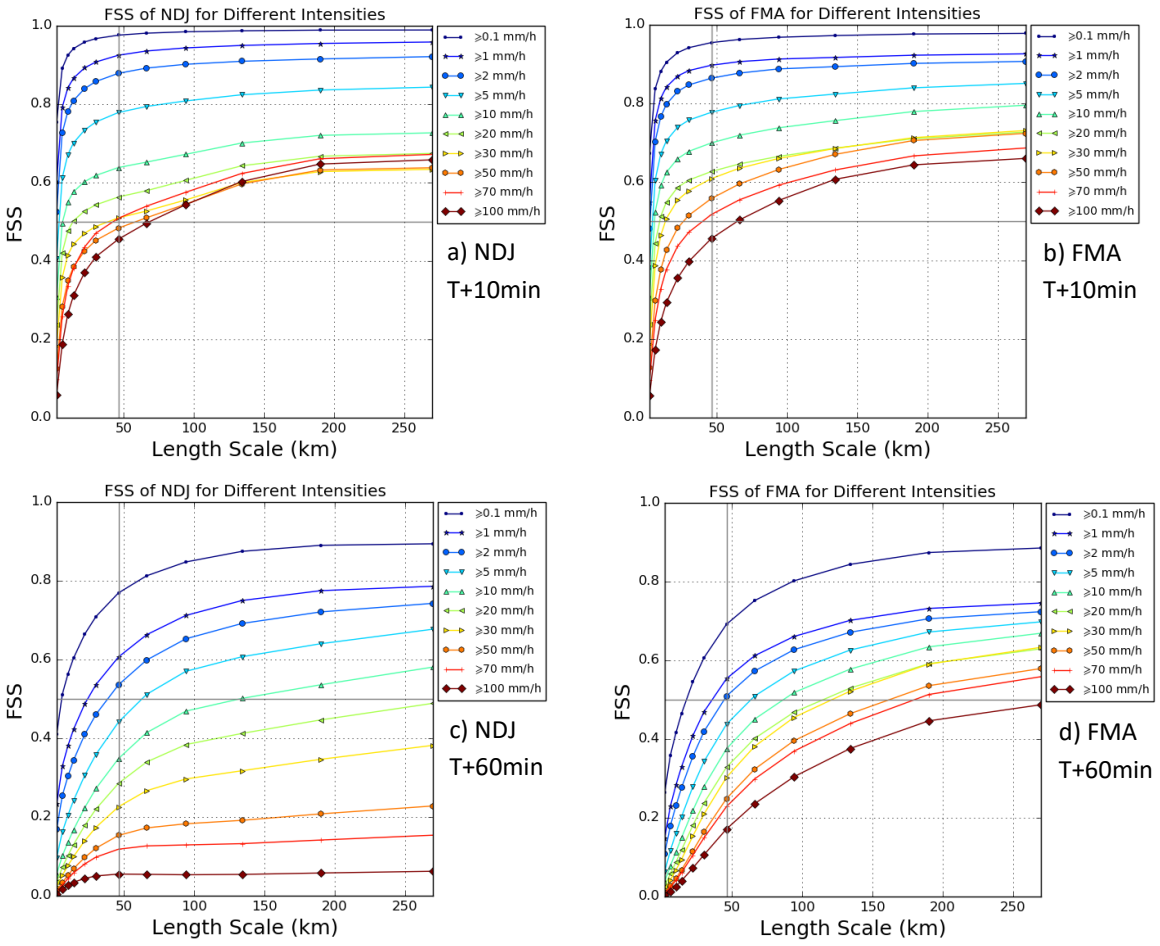

Figure 3 FSS of (a) NDJ T+10 min, (b) FMA T+10 min, (c) NDJ T+60 min and (d) FMA T+60 min.

Table 2 Thresholds (mm/h) of events with useful forecasts from ANN-NCST, based on seasons and lead times.

Season	T+10m	T+20m	T+30m	T+40m	T+50m	T+60m
NDJ	0.1/1/2/5/10/20/30	0.1/1/2/5/10/20	0.1/1/2/5/10	0.1/1/2/5	0.1/1/2	0.1/1/2
FMA	0.1/1/2/5/10/20/30/50/70	0.1/1/2/5/10/20/30	0.1/1/2/5/10	0.1/1/2/5	0.1/1/2	0.1/1/2

In order to assess how the forecast usefulness depends on the spatial sale of the phenomena, two reference lines are used in Figure 3: the FSS of 0.5 and the length scale of 46 km. In most situations FSS of 0.5 can be a good indicator of useful forecasts (Skok and Roberts 2016). The length scale of 46 km is chosen as it is the closest to the spatial scale that MSS forecasters use for evaluating heavy rain warnings; forecasters consider a heavy rainfall warning as accurate when any rain gauge has recorded heavy rain event island wide (~ 45 km). Therefore, in the context of one-hour nowcasting, a useful forecast is considered as those with FSS≥ 0.5, a length scale ≤ 46 km and a lead time ≥ 15 min.

Using the definition of a useful forecast above, Table 2 lists all the useful forecasts that the ANN-NCST can provide. Table 2 shows that for forecasts of heavy rain events (threshold ≥ 50 mm/h) the ANN-NCST can hardly provide any useful references for forecasters.

Figure 4 shows how FSS drops over lead time for various thresholds. It can be found that at small thresholds from 0.1 mm/h to 2 mm/h, FSS scores in NDJ (blue curve) is higher than FMA (red curve) but the other way around when threshold increases above 5 mm/h, and becomes comparable when the threshold reaches 70 mm/h. As there are more occurrences of rain events with larger coverage in NDJ than in FMA, a better predictability is expected for lighter rainfall due to larger

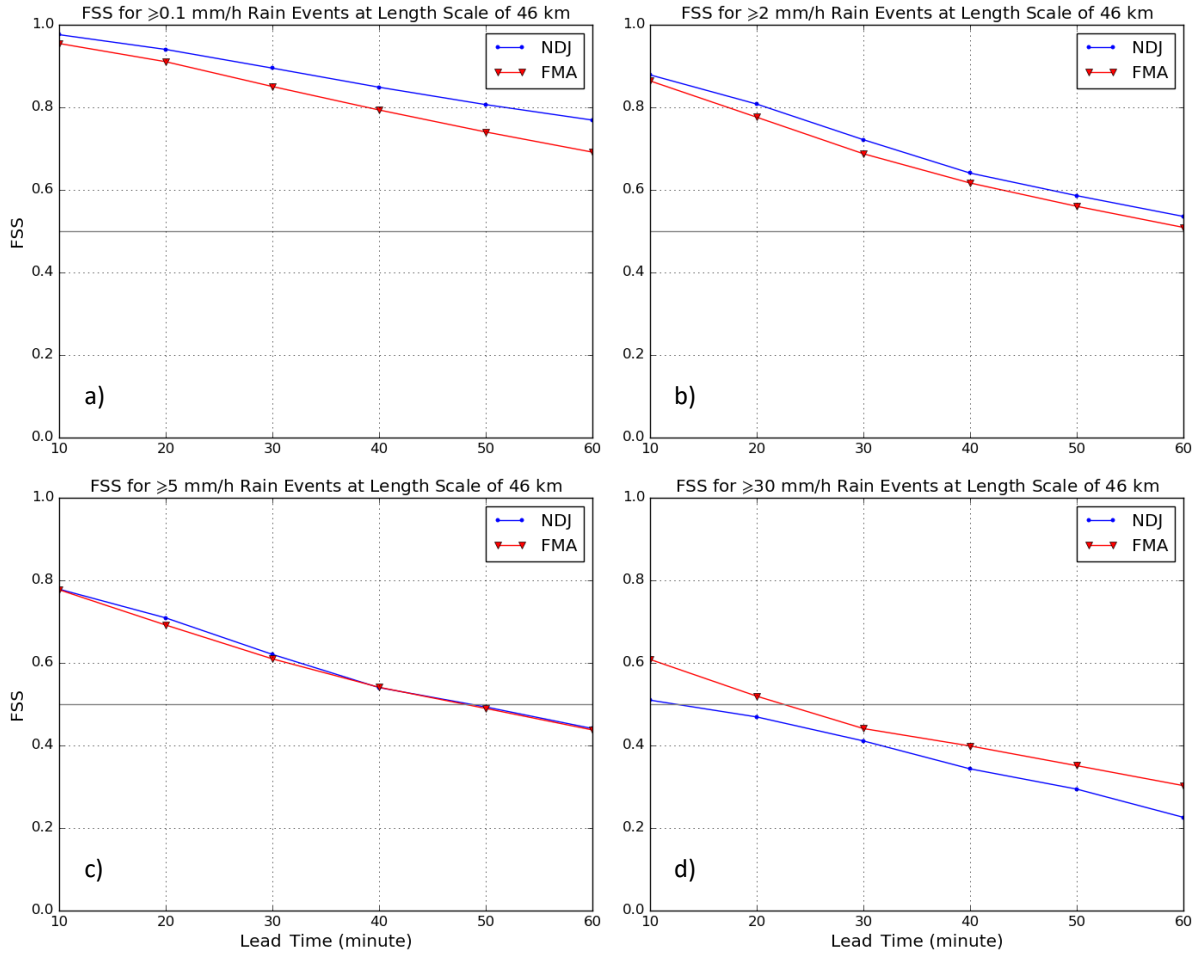

Figure 4 FSS versus lead time for length scale of 46 km for different thresholds 0.1 mm/h (a), 2 mm/h (b), 5 mm/h (c) and 30 mm/h (d).

coverage but not for heavier rainfall because of its relatively smaller fraction of total rain area in the NDJ season than in the FMA season.

For smaller domain (red and blue boxes in Figure 1) verification, scores based on contingency tables are investigated. The contingency tables are firstly derived based on Table 1 for each domain, where a 'Yes' event is defined when any grid point within the domain has a value equal to or greater than a chosen threshold, and a 'No' event is when all grid point values are less than a threshold. *POD*, *SR*, *Bias*, and *CSI* can subsequently be calculated and plotted using performance diagram as in Figure 5. Only events of ≥ 0.1 mm/h and ≥ 50 mm/h with the lead time of T+30 min (cyan boxes) and T+60 min (purple boxes) are plotted considering that 50 mm/h is the threshold for operational heavy rain warning and the scores for ≥ 0.1 mm/h basically provide the scores for rainfall locations detection only regardless of intensity.

In the performance diagram, the location of the box shows how good a forecast is in terms of *POD, SR*, *Bias*, and *CSI*. The dotted coordinate lines are metrics for *Bias* indicating under-forecast bias (below the diagonal line) or over-forecast bias (above the diagonal line); curved coordinate lines are *CSI* metrics where the upper-right corner is the best (*CSI*=1) and the lower-left corner is the worst.

As the Singapore domain and the West domain are the largest two domains, the scores over these two are the highest due to a larger neighbourhood allowance for location errors and the forecasts are also

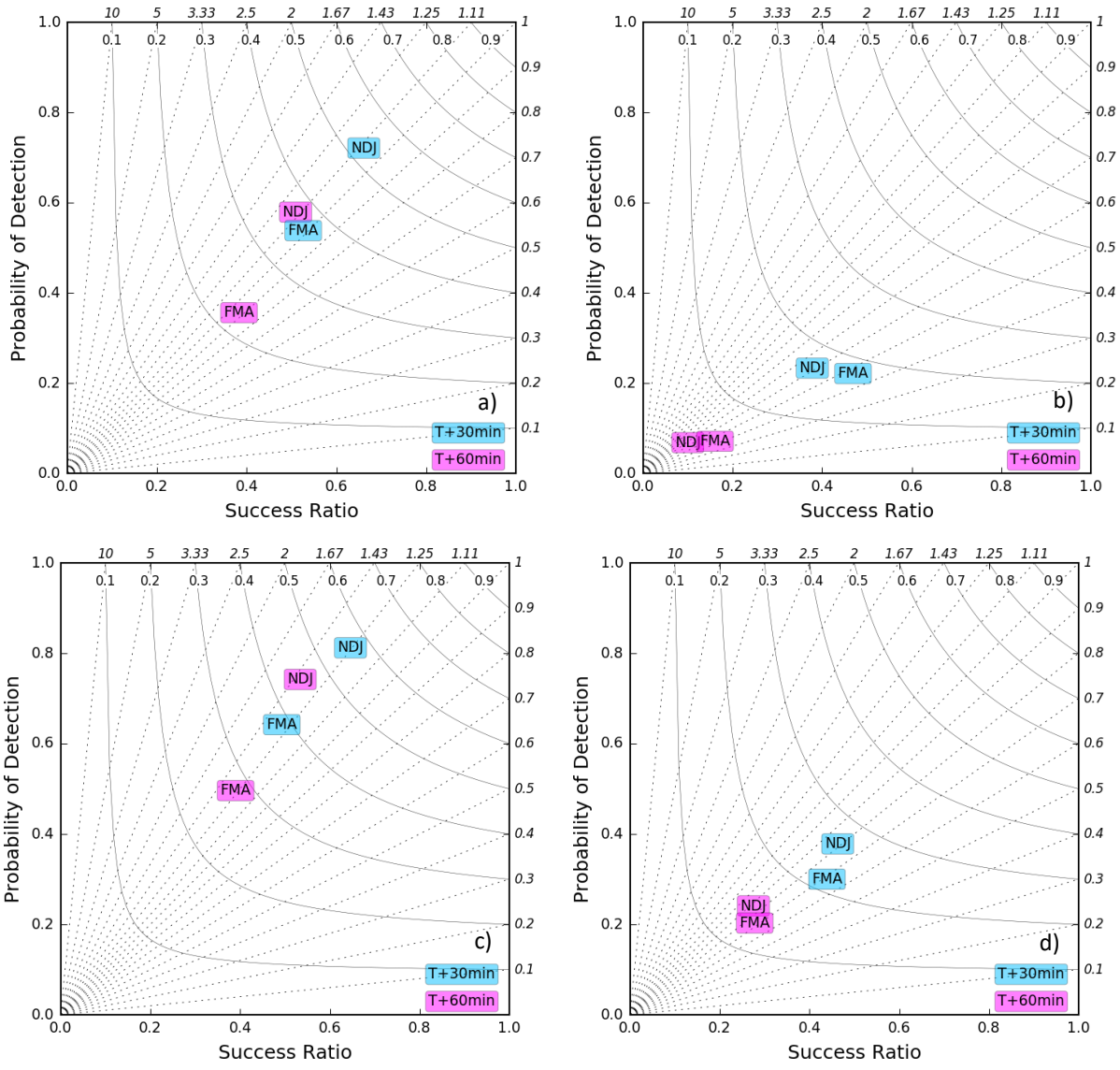

Figure 5 Performance diagram for different threshold and verification domains: (a) West domain with threshold ≥ 0.1 mm/h, (b) West domain with threshold ≥ 50 mm/h, (c) Singapore domain with threshold ≥ 0.1 mm/h and (d) Singapore domain with ≥ 50 mm/h. The curved lines indicate the *CSI*, while the dotted lines indicate the *Bias*.

the least biased compared those over the other four smaller domains (plots not shown).

From panel (d) of Figure 5 we can see that the CSI scores are not very high (between 0.2-0.3), but the forecasts have skill when compared to a reference *CSI* derived from observed base frequency (CSI_{ref}). CSI_{skill} can thus be calculated (Eq. 9) where positive CSI_{skill} indicates that there is some skill over CSI_{ref} and negative value means there is not. For simplicity, only results for forecasts of T+30 min and T+60 min are shown in Table 4 by printing out the maximum threshold for positive CSI_{skill} (thus the higher the better) with respect to lead time and domain. Table 4 shows that in general, the ANN-NCST has better performance in the NDJ season than in the FMA season for all the small domains and lead times.

Table 4. Maximum threshold (mm/h) of positive CSI skill scores with respect to lead time, domain for different seasons.

Lead Time	Season	Singapore	West	Central-North
T+30 min	NDJ	100	100	100
T+60 min	FMA	100	100	70
Lead Time	Season	Central-Central	Central-South	East
T+30 min	NDJ	100	100	100
T+60 min	FMA	30	50	100

Table 4 shows that there is no negative CSI_{skill} over the Singapore domain or West domain for all thresholds and lead times for the two seasons, suggesting the ANN-NCST can have added value over forecasts purely based on climatology for intensive rainfall up to 100 mm/h over a sub-region of Singapore when the spatial scale is no smaller than 20×20 km^2, or half the spatial scale of Singapore Island.

CONCLUSION

A nowcasting system based on ANN developed in MSS has been running in real-time since April 2017. The ANN-NCST includes two main steps: firstly, the model is trained online on past cases, and then, once trained, it provides future one-hour reflectivity forecasts at a resolution of 2 km over a 187×154 km^2 domain. The forecasts with lead times from T+15 min to T+60 min can be used to support forecasters. Two 3-month period of simulations are evaluated using metrics including *Bias*, *FSS*, and *CSI*.

Results indicate that the ANN-NCST is able to provide realistic forecasts of radar reflectivity with relatively small biases in terms of probability distribution. Considering the verification over the entire domain (187×154 km^2), the ANN-NCST forecasts have been shown to be useful (a forecast has been judged useful if FSS≥ 0.5) for light rain events with threshold less than 5 mm/h. For precipitation intensities higher than 5 mm/h, a poorer performance is observed in the NDJ season than in the FMA season. We suppose this is related to the fitting algorithm implemented in the training module and it is worth more investigation and can be improved in the future. Over verification domains smaller than 46×46 km^2, scores based on the contingency table show that the ANN-NCST demonstrates the capability to outperform climatology for heavy rain events over a domain with dimensions up to 20×20 km^2, but the usefulness of this product to operations has not been investigated.

In the future, the plan is to test the use of ANN-NCST forecasts to assist heavy rain warnings in a relatively small domain of Singapore Island and the immediate vicinity.

ACKNOWLEDGMENTS

We thank our colleagues Chee Kiat Teo and Joshua Qian for providing helpful suggestions and thank Ryan Kang, Kai Yuan Zheng, and Jia Yan Huang for sharing their knowledge and experiences in heavy rain warning issuance and verification.

REFERENCES

Chang C.P., Lu, M.M., Lim, H. (2016) Monsoon Convection in the Maritime Continent: Interaction of Large-Scale Motion and Complex Terrain. *Meteorological Monographs*, 56:6.1–6.29.

Dixon, M.J., Wiener, G. M. (1993) TITAN: Thunderstorm identification, tracking, analysis, and nowcasting – a radar-based methodology. *Journal of Atmospheric and Oceanic Technology*, 10:785–797.

Fong, M. (2012) The Weather and Climate of Singapore. Ng, L.K. (Ed.), Meteorological Service Singapore, Singapore, pp. 72,81,153–159.

Kumar, L. S., Lee, Y. H., Yeo, J. X., Ong, J. T. (2011) Tropical Rain Classification and Estimation of Rain from Z-R (Reflectivity-Rain Rate) Relationships. *Progress in Electromagnetics Research*, 32:107–127.

Li, P. W., Lai, E. S. T. (2004) Short-range quantitative precipitation forecasting in Hong Kong. *Journal of Hydrology*, 288:189–209.

Mandapaka, P. V., Qin, X. (2013) Analysis and Characterization of Probability Distribution and Small-Scale Spatial Variability of Rainfall in Singapore Using a Dense Gauge Network. *Journal of Applied Meteorology and Climatology*. 52: 2781–2796.

McCulloch, W. S., Pitts, W. (1943) A logical calculus of the ideas immanent in nervous activity. *Bulletin of Mathematical Biology*, 5:115–133.

Mittermaier, M., Roberts, N. (2010) Intercomparison of Spatial Forecast Verification Methods: Identifying Skillful Spatial Scales Using the Fractions Skill Score. *Weather and Forecasting*, 25: 343–354.

Mittermaier, M. P. (2014) A Strategy for Verifying Near-Convection-Resolving Model Forecasts at Observing Sites. *Weather and Forecasting*, 29: 185–204.

Pedregosa, F., Varoquaux, G., AGramfort, A., Michel, V., Thirion, B., Grisel, O., Blondel, M., Prettenhofer, P., Weiss, R., Dubourg V., et al. (2011) Scikit-learn: Machine Learning in Python. *Journal of Machine Learning Research*, 12: 2825–2830.

Qian J. H. (2008) Why Precipitation Is Mostly Concentrated over Islands in the Maritime Continent. *Journal of the Atmospheric Sciences*, 65: 1428–1441.

Reyniers, M. (2008) Quantitative Precipitation Forecasts Based on Radar Observations: Principles, Algorithms and Operational Systems. Royal Meteorological Institute of Belgium. Available at: www.meteo.be/meteo/download/fr/3040165/pdf/rmi_scpub-1261.pdf, last accessed: 25 May 2018.

Roberts, N. M., Lean, H. W. (2008) Scale-Selective Verification of Rainfall Accumulations from High-Resolution Forecasts of Convective Events. *Monthly Weather Review*, 136: 78–97.

Skok, G., Roberts, N. (2016) Analysis of Fractions Skill Score properties for random precipitation fields and ECMWF forecasts. *Quarterly Journal of the Royal Meteorological Society*, 142: 2599–2610.

Sun, J., Xue, M., Wilson, J.W., Zawadzki, I., Ballard, S.P., Onvlee-Hooimeyer, J., Joe, P., Barker, D.M., Li, P., Golding, B., et al. (2014) Use of NWP for Nowcasting Convective Precipitation: Recent Progress and Challenges. *Bulletin of the American Meteorological Society*, 95: 409–426.

GLOSSARY

Automatic weather stations (AWS): Weather stations that collects, stores, and transmits automatically various weather information (e.g. rainfall, temperature).

Artificial Neural Network: A computer system framework with a number of nodes or 'neurons', potentially with many layers of nodes, that alter the input data to produce output data.

ANN-based Nowcasting system (ANN-NCST): The nowcasting system developed at MSS, based on artificial neural network using radar reflectivity.

Bias (based on the contingency table): compares the number of forecasted events with the number of observed events.

Boreal: Refers to the north, often used to refer to the Northern Hemisphere.

Climate Hazards Group InfraRed Precipitation with Stations (CHIRPS): near-global gridded rainfall dataset developed by the US Geological Survey and the University of California, Santa Barbara.

Coefficient of correlation (*r*): The strength of a linear relationship between two variables (if plotted on a graph, how closely the points fit to a straight line).

Cold surges: strong northeast winds over the South China Sea that bring increased convection over the Maritime Continent, usually occurring during the Northeast Monsoon.

Cold spell: A period of abnormally cold temperatures relative to the normal temperature for the region.

Contingency table: A table that summarises the distribution of two variables, in this case the forecast and observed conditions, and is used to study the correlation between these variables. Various metrics include Bias, CSI, POD, SR.

Cool spell: A period of abnormally cooler temperatures for the region (but not as cold as cold spell).

Correlation of anomalies (CORA): A measure of the linear association between predicted and observed anomalies, also termed 'anomaly correlation coefficient'. Similar to *r*, but when the variables are specifically anomalies and generally applied to a spatial field.

Critical Success Index (CSI): Similar to POD, although it also considers the number of false alarms (there by penalising for both false alarms and missed events).

Decadal variability: Variations in the climate that occur on the time scale of 10 to 30 years.

European Centre for Medium-range Weather Forecasts (ECMWF): A research institute and operational service dedicated to improve forecasts in the 7 to 15-day window that provides additional forecasts, including those at the subseasonal to seasonal timescale.

El Niño–Southern Oscillation (ENSO): Irregular variations in the winds and sea surface temperatures over the tropical Pacific Ocean (variations in the Walker Circulation). The pattern oscillates between neutral, El Niño, and La Niña with no regular pattern.

Fractions Skill Score (FSS): Used to verify forecasts over an area. Dividing the study area into a grid, the FSS compares the number of positive forecasts in a region (or 'neighbourhood') around each grid box with how many positive events were observed in that same region. Positive forecasts/events are often grid boxes with rainfall above a certain threshold.

Indian Ocean Dipole (IOD): The difference in sea surface temperature between the western Indian Ocean (Arabian Sea) and the eastern Indian Ocean (south of Indonesia), which oscillates irregularly.

Inter-monsoon (IM): The transitional periods between the monsoons seasons: Northeast and Southwest.

Intertropical Convergence Zone (ITCZ): A belt of low pressure near the equator where the trade winds from the Northern and Southern hemispheres meet, generally marked by intense convection and rainfall.

Inverse Distance Weighting (IDW): An interpolation method, where the unknown value at a particular point is combination of nearby known values, with the proportion, or weight, given to each known-value based on its distance from unknown-value point.

IRI Data Library (IDL): An online data repository and analysis tool.

Machine-Learning: Where computer systems, using algorithms and statistical models, progressively improve their performance for a specific task.

Madden-Julian Oscillation (MJO): One of the most important and identified fluctuations in tropical weather on weekly to monthly timescales. It is often characterised as a pulse of cloud and rain that moves eastward along the equator, typically occurring every 30–60 days.

Mean absolute error (MAE): Used for verification of forecasts, it is the average size of the forecast error.

Mean relative error (MRE): Similar to above; the average size of the forecast error compared to the actual values.

Mean square skill score (MSSS): Used for verification of deterministic forecasts. The score compares the mean square error when using the forecasts with that of the mean square error of the climatology.

Ministry of the Environment and Water Resources (MEWR): Ministry in Singapore that is committed to providing Singaporeans with a quality living environment. The two statutory boards associated with MEWR are: National Environment Agency (NEA; with meteorological services under MSS); and Singapore's National Water Agency (PUB).

Nino3.4: Index used to measure ENSO, based on sea surface temperatures in the tropical eastern Pacific.

Northeast (NE): Generally referring to the wind direction, or monsoonal flow during the boreal winter.

Nowcasting: Current weather conditions or a forecast of how these observed conditions may change in 0 to 2 hours (very near future).

Numerical Weather Prediction (NWP): Computer models that solve mathematical equations representing atmospheric physics. Used extensively in weather forecasting.

Probability of detection (POD): Based on the contingency table, the fraction of the observed events that were correctly forecasted.

Python: General purpose programming language, in which code readability is important.

Radar reflectivity: The amount of radiant-energy sent out by a radar that is reflected back (a potentially useful proxy for precipitation amount).

Root mean squared error (RMSE): The square root of the MSE.

Southwest (SW): Generally referring to the wind direction, or monsoonal flow during the boreal summer.

Subseasonal to seasonal (S2S) forecasts: Forecasts between the weather timescale and seasonal timescale, often considered to be forecasts for two weeks to two months into the future.

Success Ratio (SR): Based on the contingency table, the fraction of the forecasted events that were also observed.

Tropical Rainfall Measuring Mission (TRMM): A gridded rainfall dataset based on satellite imagery.

World Climate Research Programme (WCRP): An international programme to facilitate the analysis and prediction of Earth system variability and change.

World Meteorological Organisation (WMO): An agency under the United Nations for meteorology, both weather and climate, as well as operational hydrological services.

World Weather Research Programme (WWRP): WMO research programme that focuses on high-impact weather.

Website: ccrs.weather.gov.sg

Address: 36 Kim Chuan Road, Singapore